Delayed Freshwater Export from a Greenland tidewater glacial fjord

Delayed Freshwater Export from a Greenland tidewater glacial fjord

Robert Sanchez,[a] Donald Slater,[b] and Fiammetta Straneo,[a]

[a] *Scripps Institution of Oceanography, UC San Diego, San Diego, California*

[b] *School of Geosciences, University of Edinburgh, Edinburgh, United Kingdom*

Corresponding author: Robert Sanchez, rmsanche@ucsd.edu

Early Online Release: This preliminary version has been accepted for publication in *Journal of Physical Oceanography*, may be fully cited, and has been assigned DOI 10.1175/JPO-D-22-0137.1. The final typeset copyedited article will replace the EOR at the above DOI when it is published.

ABSTRACT: Freshwater from the Greenland Ice Sheet is routed to the ocean through narrow fjords along the coastline where it impacts ecosystems both within the fjord and on the continental shelf, regional circulation, and potentially the global overturning circulation. However, the timing of freshwater export is sensitive to the residence time of waters within glacial fjords. Here, we present evidence of seasonal freshwater storage in a tidewater glacial fjord using hydrographic and velocity data collected over 10 days during the summers of 2012 and 2013 in Saqqarleq (SQ), a mid-size fjord in West Greenland. The data revealed a rapid freshening trend of -0.05 ± 0.01 g/kg/day and -0.04 ± 0.01 g/kg/day, in 2012 and 2013, respectively, within the intermediate layer of the fjord (15–100 m) less than 2.5 km from the glacier terminus. The freshening trend is driven, in part, by the downward mixing of outflowing glacially-modified water near the surface and increasingly stratifies the fjord from the surface downwards over the summer melt season. We construct a box model which recreates the first-order dynamics of the fjord and describes freshwater storage as a balance between friction and density-driven exchange outside the fjord. The model can be used to diagnose the timescale for this balance to be reached, and for SQ we find a month lag between subglacial meltwater discharge and net freshwater export. These results indicate a fjord-induced delay in freshwater export to the ocean that should be represented in large-scale models seeking to understand the impact of Greenland freshwater on the regional climate system.

Accepted for publication in *Journal of Physical Oceanography*. DOI 10.1175/JPO-D-22-0137.1

1. Introduction

Mass loss from the Greenland Ice Sheet is predicted to accelerate during the 21st century, further contributing to sea level rise and with downstream consequences on ocean circulation and ecosystems (Bamber et al. 2019; Goelzer et al. 2020; Böning et al. 2016; Frajka-Williams et al. 2016; Arrigo et al. 2017; Oksman et al. 2022). Freshwater fluxes from the ice sheet are discharged in the form of both solid and liquid forms contributing cumulatively 7700 ± 460 km^3 and 8400 ± 1680 km^3 of freshwater respectively, from 2000–2016 (Bamber et al. 2018). The freshwater and its dissolved and particulate chemical content are released into long and narrow fjords before being routed onto the continental shelves where they can affect regional circulation, salinity, biogeochemistry and potentially large-scale deep convection, although recent evidence suggests Greenland's freshwater might remain close to the coast (Straneo and Cenedese 2015; Böning et al. 2016; Frajka-Williams et al. 2016; Thornalley et al. 2018; Hendry et al. 2021; Le Bras et al. 2021). The freshwater from glaciers also impacts regional ecosystems through both the direct injection of nutrients and the upwelling of ambient deep nutrients leading to highly productive fjords and fisheries (Cape et al. 2019; Meire et al. 2016a,b, 2017; Hopwood et al. 2020) that are, therefore, sensitive to future changes in freshwater fluxes (Hopwood et al. 2018; Oliver et al. 2020). The impact of freshwater will vary depending on how, when and where it mixes with seawater. This mixing is in turn affected by fjord circulation and stratification (Mortensen et al. 2011, 2020). Therefore, determining how fjord dynamics alter the distribution and export of freshwater is crucial to understanding the impact of the Greenland Ice Sheet on the ocean and ecosystems.

The liquid component of freshwater enters fjords in three forms: (i) through direct melting of ice by the ocean (submarine meltwater; SMW), (ii) meltwater from the ice sheet surface that has drained to the ice sheet base and enters the fjord from beneath a glacier (subglacial meltwater discharge; SGD), and (iii) meltwater from the ice sheet surface that has not drained to the base and enters the fjord at the surface (meltwater runoff). Since it is expected that the majority of surface meltwater does drain to the ice sheet base in this system, and since this study excludes the surface layers of the fjord, we here make no further mention of meltwater runoff. SMW fluxes are sensitive to ocean heat and released at various depths along the face of the terminus. Additionally, SMW is produced by melting icebergs as they transit through the fjord. Meltwater drained as SGD is buoyant and produces turbulent plumes which entrain ambient water and drive a strong

Accepted for publication in *Journal of Physical Oceanography*. DOI 10.1175/JPO-D-22-0137.1

overturning circulation within the fjord (Straneo and Cenedese 2015; Carroll et al. 2017). This overturning circulation, along with tidal flows and shelf-forced fluctuations, drives horizontal and vertical mixing within the fjord and determines the exchange of freshwater with the shelf (Zhao et al. 2021). However, the transport and outflow depth of the SGD plume is sensitive to fjord stratification, resulting in a complex feedback between fjord circulation and freshwater content (De Andrés et al. 2020).

Glacial fjords are often described as being in one of two states, a winter state with decreased stratification and a shelf-influenced circulation, and a summer state with increased stratification and a strong plume-driven circulation (Jackson and Straneo 2016; Gladish et al. 2014; Mortensen et al. 2014). These dramatic differences in circulation and stratification can lead to a seasonal description of glacial fjords that overlooks the dynamic evolution of fjords within a season. Additionally, the challenges of obtaining measurements in ice-congested fjords often limit field campaigns to short-duration summer surveys (Stevens et al. 2016; Beaird et al. 2015, 2017; Cape et al. 2019; Motyka et al. 2011; Wood et al. 2018; Moon et al. 2018; Inall et al. 2014; Bendtsen et al. 2015, 2021; Muilwijk et al. 2022). While these surveys provide invaluable snapshots of heat, nutrient, and meltwater fluxes, it is often assumed that the data are representative of the whole summer and some heat budgets explicitly assume the fjord is in a "steady state" or use a single summer average (Inall et al. 2014; Jackson and Straneo 2016).

However, a limited number of observations have shown significant subseasonal variability of hydrographic properties in fjords (Stuart-Lee et al. 2021; Carroll et al. 2018; Mortensen et al. 2014, 2013, 2018; Meire et al. 2016b; Mernild et al. 2015). For example, Mortensen et al. (2011, 2014, 2018) show that Godthåbsfjord freshens and the isopycnals deepen throughout the summer, suggesting that fjord processes modulate the timing and vertical distribution of freshwater export. This is in contrast to the approach of large-scale ocean models, which often input freshwater from glacial freshwater at the surface and assume the transit time of meltwater through fjords is negligible (Arrigo et al. 2017; Dukhovskoy et al. 2019). To further understand the subseasonal evolution of glacial fjords and their impact on freshwater export, we use a dataset of high-frequency hydrographic and velocity observations collected over 10 days during each of the summers of 2012 and 2013 in Saqqarleq (previously known as Sarqardleq Fjord), a mid-size fjord in west Greenland associated with Saqqarliup Sermia glacier. The data revealed a rapid freshening trend of 0.05

Accepted for publication in *Journal of Physical Oceanography*. DOI 10.1175/JPO-D-22-0137.1

g/kg/day and 0.04 g/kg/day, in 2012 and 2013 respectively, within the intermediate layer of the fjord less than 2.5 km from the glacier. These freshening trends were of similar magnitude despite the fact that 2012 was a year of record surface melt and 2013 was an average melt year. The freshening indicates that SMW and SGD from the glacier is stored within the fjord leading to a transformation of fjord waters and a delay in the net export of freshwater. A box model is developed to elucidate the storage and release dynamics of the glacial fjord. The box model is formulated for Saqqarleq, but is generic and can be applied to other systems. Our results suggest that Greenland's glacial fjords are nonsteady and respond rapidly to the input of ice sheet meltwater. The freshwater storage results in a lag of peak freshwater export from the glacier to the ocean that needs to be accounted for in any regional or global ocean model that does not resolve fjords and fjord processes.

2. Setting, Data and Methods

a. Setting and Background

We investigate changes within Saqqarleq (SQ), a mid-sized glacial fjord in west Greenland associated with the glacier Saqqarliup Sermia, during a period of sustained SGD. SQ is the southern arm of the Ilulissat Isfjord system which connects Sermeq Kujalleq (commonly referred to as Jakobshavn Isbrae) with Disko Bay (Fig. 1a). SQ has a broad sill (S1) about 500 m from the grounding line isolating the glacier from the deepest SQ waters. This sill varies in depth from 50 m at its southwest end to 100 m at its deepest point. The fjord varies in width from about 6 km at the head of the fjord, to 2.2 km in the main channel of the fjord before it connects to Tasiusaq (TQ) and then Ilulissat Isfjord. SQ and TQ are separated by an 80 m deep sill (S2) that is 16 km downfjord of Saqqarliup Sermia, and TQ is separated from Ilulissat Isfjord by a 125 m deep sill (S3). The sill between TQ and Ilulissat prevents the deeper relatively warm basin waters of Ilulissat from reaching SQ.

SQ lacks a thick ice mélange, unlike major glacial fjords such as Ilulissat Isfjord and Sermilik, which enables measurements to be made within 200 m of the terminus and makes SQ ideal for field studies of ice-ocean interactions (Stevens et al. 2016; Mankoff et al. 2016; Slater et al. 2018; Wagner et al. 2019; De Andrés et al. 2020). SGD enters the fjord from below the glacier at two locations, a primary plume located 2.3 km along the terminus from the southwest corner and a secondary plume 4.5 km along the terminus [Fig. 1c, (Stevens et al. 2016)]. The secondary plume

Accepted for publication in *Journal of Physical Oceanography*. DOI 10.1175/JPO-D-22-0137.1

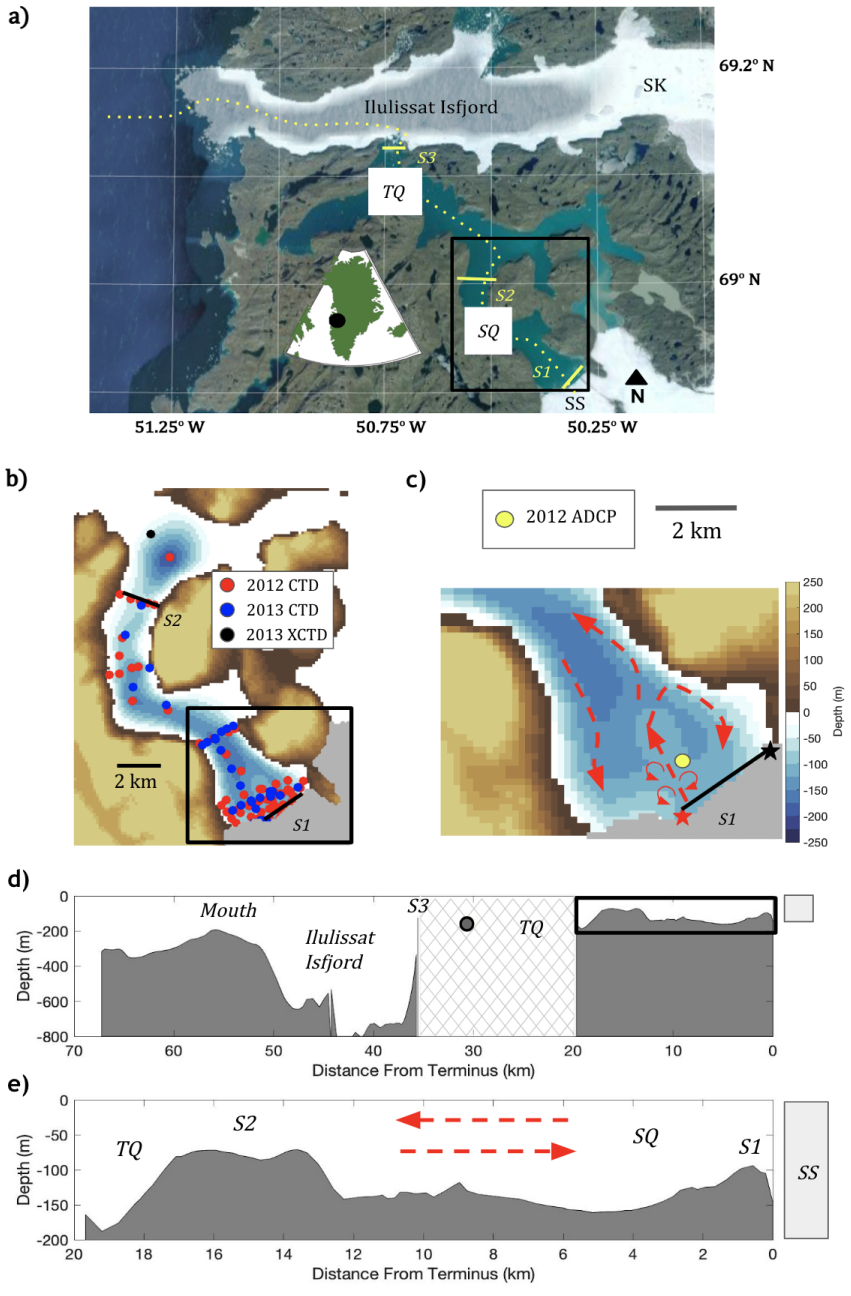

FIG. 1. a) A regional map of Saqqarleq (SQ), Tasiusaq (TQ) and Ilulissat Isfjord showing sill locations and nearby glaciers Saqqarliup Sermia (SS) and Sermeq Kujalleq (SK). The inset map shows the location of SQ within the Greenland continent. The yellow dashed line is the bathymetry slice shown in (d) and (e). b) Map of SQ with the locations of CTDs in 2012 (red), 2013 (blue) and a 2013 XCTD (black). c) Near-terminus bathymetry and a schematic of the circulation. Locations of the primary plume (red star) and secondary plume (black star) based on Stevens et al. (2016) and location of moored ADCP (Fig. 7). d) Along-track bathymetry profile created using BedMachinev3 (Morlighem et al. 2017). Cross hatching fills the region where data is unreliable. A circle marks the single depth point available (2013 XCTD). e) A close-up of SQ, with overturning schematic.

Accepted for publication in *Journal of Physical Oceanography*. DOI 10.1175/JPO-D-22-0137.1

is associated with substantially weaker SGD resulting in a deeper neutral buoyancy depth (Stevens et al. 2016; De Andrés et al. 2020). A remote-control kayak equipped with a depth-varying CTD sampled within the surface expression of the primary plume in 2013, finding that the plume was composed of 90% entrained ambient water, 10% SGD and less than 0.1% SMW (Mankoff et al. 2016). Along-fjord transects of temperature and velocity revealed that after surfacing, the plume submerged and flowed out as a subsurface jet (Mankoff et al. 2016). A high-resolution simulation of SQ, constrained with observations from 2013, found that the plume-turned-jet impinged on the fjord wall and generated a vigorous terminus-scale wide recirculation generating widespread melting of the glacier terminus [Fig. 1c, (Slater et al. 2018)].

Previously, De Andrés et al. (2020) used parts of this dataset to explore differences in the surface emergence of a subglacial plume across two consecutive years, including one in a year with record SGD (2012). They found that greater cumulative SGD was associated with increased fjord stratification which, in turn, exerted a dominant influence on plume height. They did not investigate, however, the physical mechanisms controlling the stratification and the potential impacts this stratification has on the export of freshwater.

b. Data

Conductivity, Temperature and Depth (CTD) profiles were collected from a small boat in the fjord from 17–27 July in 2012 and 23 July – 1 August 2013 (Fig. 1b). The profiles were collected using an RBR XR 620 CTD and averaged into 1 dbar bins. 90 casts were collected in 2012 and 96 casts were collected in 2013. In 2012 (2013), 51 (59) of the casts extended to at least 100 m and only these deeper casts were used in our hydrographic analysis. Additionally in 2013, a Sippican eXpendable CTD (XCTD) was collected just outside the 80 m deep S2 in TQ. The data are presented in Conservative Temperature (Θ or temperature), Absolute Salinity (S or salinity) and Potential Density [ρ or density; (McDougall and Barker 2011)] with stratification defined using the Brunt-Väisälä frequency

$$N^2 = -\frac{g}{\rho_{ref}} \frac{\mathrm{d}\rho}{\mathrm{d}z}, \tag{1}$$

where g is gravitational acceleration and $\rho_{ref} = 1026$ kg/m^3 is a reference density.

Accepted for publication in *Journal of Physical Oceanography*. DOI 10.1175/JPO-D-22-0137.1

An upward-looking moored Teledyne RDI 300 kHz Acoustic Doppler Current Profiler (ADCP) was deployed 1.6 km from the terminus (Fig. 1c) and collected velocity data from July 2012 – April 2013. The ADCP was deployed on the seafloor at 114 m and recorded velocity in 4 m bins from 10–106 m, after removing the top two bins for side-lobe effects. The barotropic tide was estimated from a pressure sensor, the Arctic Ocean Inverse Tide Model (Padman and Erofeeva 2004; Erofeeva and Egbert 2020) when data was unavailable, and subtracted from the ADCP data (Sup. Fig. 1). The estimates of SGD entering the fjord are taken from the Modele Atmospherique Regional [MAR;(Fettweis et al. 2017; Delhasse et al. 2020)] with the dataset provided by Mankoff et al. (2020). We also use salinity values collected from seals as reported in Mernild et al. (2015) and calibrate them against our CTD data (Sup. Fig. 2).

3. Analysis of Observational Data

a. Background Hydrography

The hydrography of SQ has been investigated by De Andrés et al. (2020) and Stevens et al. (2016), but a brief description is necessary here to provide context for our analysis. During summer, the fjord can be approximated as a three-layer system with a surface layer approximately 10–15 m deep, an intermediate layer between 15–100 m deep and a homogeneous layer deeper than 100 m (BW, Fig. 2). Temperature profiles (Fig. 2a), reveal a warm surface layer, presumably from solar heating, and a colder layer extending from 15 m to the bottom. There is little difference in temperature between the second and third layer. Interannual differences between 2012 and 2013 are small with mean temperatures below the surface layer of 0.9 °C and 1 °C respectively. Salinity profiles (Fig. 2b), show that the intermediate layer of the fjord is substantially fresher in 2012 (mean salinity 31.9 g/kg) than in 2013 (32.9 g/kg). The interannual differences in salinity are consistent with 2012 being a year of record ice sheet surface melt (Nghiem et al. 2012; Tedesco et al. 2013). Below 100 m in the basin layer, the salinity between the two years are similar. This evidence suggests that S1 blocks the majority of glacial water from reaching the basin layer and that BW is primarily composed of waters unmodified by SS and imported from outside of the fjord, similar to the deep basin waters of some shallow-silled glacial fjords (Hager et al. 2022). This basin water has characteristics of diluted Baffin Bay Polar Water, one of the two water masses

Accepted for publication in *Journal of Physical Oceanography*. DOI 10.1175/JPO-D-22-0137.1

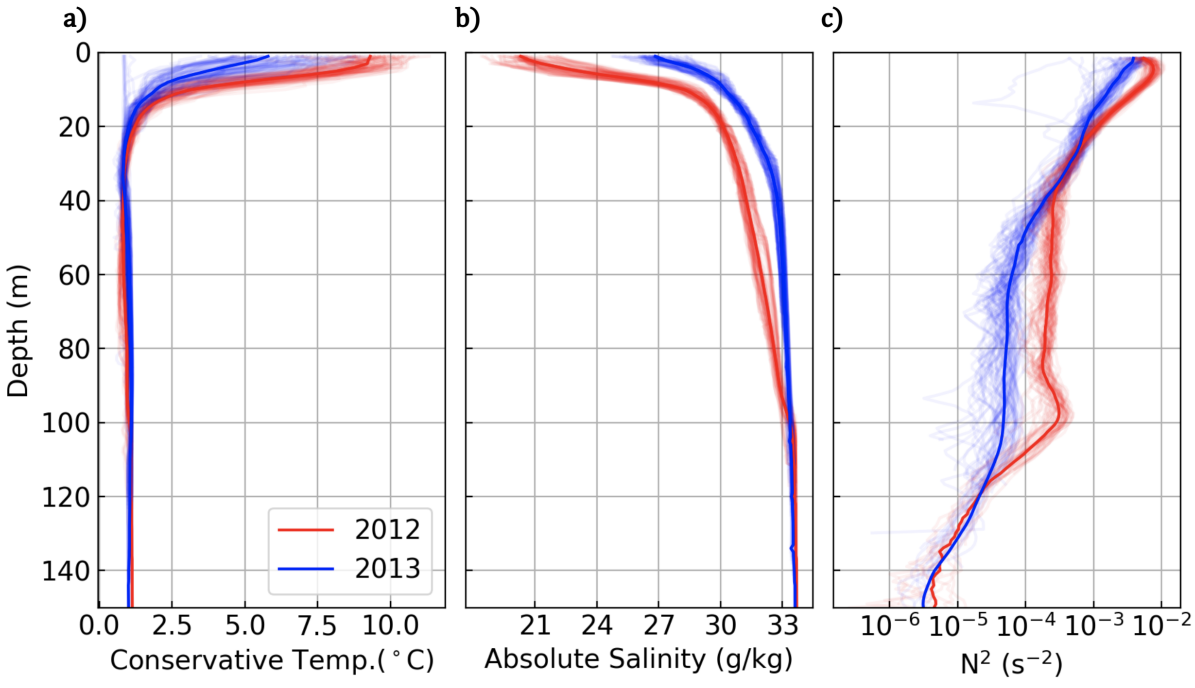

FIG. 2. a) Conservative Temperature versus depth (red 2012, blue 2013). b) Absolute Salinity. c) Stratification (N^2) over the top 150 m. In all profiles the mean profile is given in bold. The stratification profiles are low-pass filtered over a window of 10 m to remove noise. The x-axis in panel c is logarithmic.

found in Greenland north of Davis Strait (Gladish et al. 2014; Stevens et al. 2016; Rysgaard et al. 2020; Mortensen et al. 2022).

The density in SQ is dominated by salinity, and the stratification profiles reveal that decreased salinity above 100 m is associated with increased vertical density gradients (Fig. 2). In both years, the stratification exhibits peaks around the surface layer but decreases with depth. Above 40 m, the mean stratification was approximately double in 2012 (2×10^{-3} s^{-2}) compared to 2013 (1×10^{-3} s^{-2}). The mean stratification between 40 to 100 m is about 4 times higher in 2012 (2.7×10^{-4} s^{-2}) compared to 2013 (0.07×10^{-4} s^{-2}). The profiles in 2012 also exhibit a peak in stratification just above the homogeneous layer (100 m) before converging to the 2013 properties reflecting the presence of sill S2.

Accepted for publication in *Journal of Physical Oceanography*. DOI 10.1175/JPO-D-22-0137.1

b. Continuous Fjord Freshening

We find that SQ gets fresher during the summer field campaign in both years indicating it is not in steady state. We analyze freshwater storage by examining temporal trends in salinity within layers of the fjord. We focus on the intermediate layer (15–100 m depth) because the surface layer shows a high degree of variability, presumably, imparted by processes that are not the focus of this study, such as runoff (meltwater, land and precipitation) and solar insolation (Sup Fig. 4). While these surface processes are important, strong stratification ($N^2 \approx 10^{-2}$ s^{-2}) likely limits their impact at depth in this system. In both 2012 and 2013, the mean salinity over the intermediate layer continuously decreased over the course of each field campaign (Fig. 3). The mean salinity also exhibited an along-fjord trend with fresher waters closer to the glacier, but the temporal trend is greater than the longitudinal trend. We can thus rule out that the freshening is due to the advection of freshwater from Ilulissat Isfjord as otherwise the salinity gradient would be reversed. The freshening trend in 2012 is -0.05 ± 0.01 g/kg/day (r^2 = 0.77) and in 2013 is -0.04 ± 0.01 g/kg/day (r^2 = 0.74), with uncertainty defined using a bootstrapping method. This trend is consistent with a moored CTD at 70 m that recorded salinity continuously over this time period (Sup. Fig. 3). The CTD data is concentrated near the head of SQ where mixing is likely to be most intense (Bendtsen et al. 2021), and therefore it is unclear how close to the shelf the freshening trend persists. The jet from the glacier outflows at around 20 m depth, but the freshening occurs at all depths (Sup. Fig. 4) suggesting that either the outflowing freshwater is being vertically mixed downwards or strong submarine melting is freshening waters at all depths.

c. Subglacial Meltwater Discharge is the Dominant Freshwater Source

Next, we show that the freshening trend is due to an increase in SGD content in the water column. We can visually identify which freshwater source is responsible using a temperature and salinity (TS) diagram with the depths 25 m, 40 m, 80 m and 100 m highlighted in Figure 4. The profiles shown are representative of the start, middle and end of the field campaign and were all collected from approximately the same distance from the glacier. By looking at the change in temperature associated with freshening we can determine the source of freshwater. For example, we expect freshening driven by SMW to be associated with a substantial cooling of water while freshening due to SGD is associated with a much smaller change in temperature. In 2012, the change in

Accepted for publication in *Journal of Physical Oceanography*. DOI 10.1175/JPO-D-22-0137.1

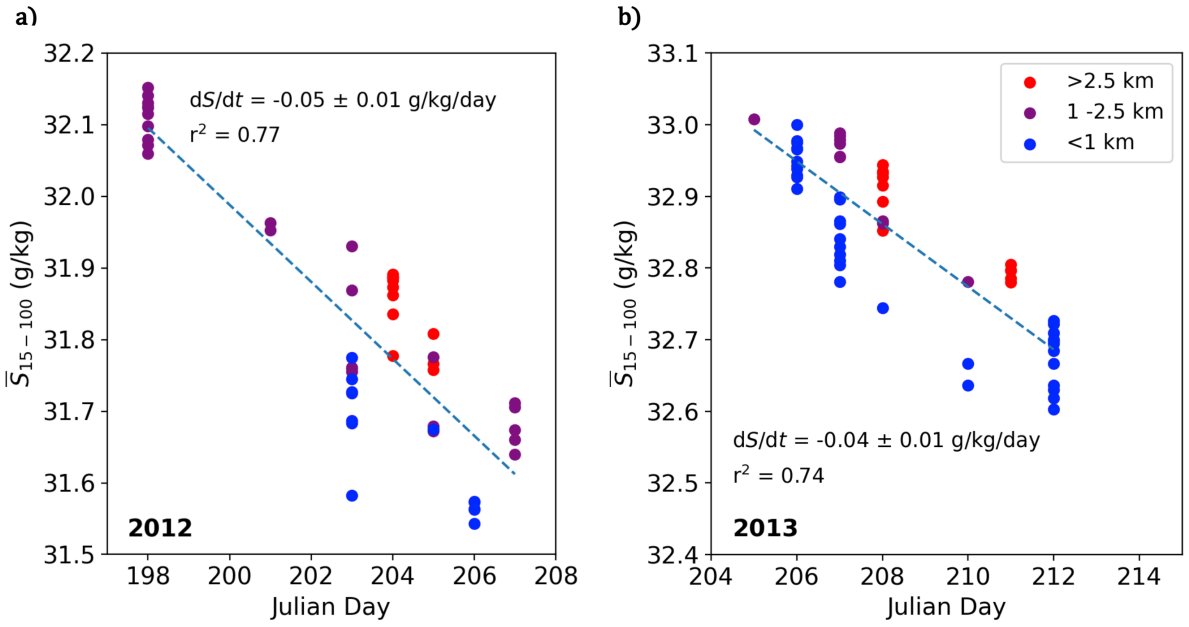

FIG. 3. a) Mean Absolute Salinity of 2012 CTD profiles from 15–100 m (surface layer to S2 depth) with a best fit trend. Colors indicate distance from terminus. X-axis is the Julian day. b) same but for 2013.

properties at each depth are roughly parallel to the subglacial meltwater discharge-mixing line indicating that the freshening is due to an increase in SGD at depth rather than SMW. However in 2013, only the properties at 25 m appear parallel to the subglacial meltwater discharge-mixing lines while deeper water appears to be on a slope between the subglacial meltwater discharge-mixing line and the submarine melt line. Following the procedure of Mankoff et al. (2016) and Mortensen et al. (2020) (see Supplemental) we use a water-mass analysis to quantify changes in the relative concentration of SGD and SMW (Table 1). The fraction of SGD significantly increased by around 1% in both years ($p < 10^{-4}$ for all cases). Changes in the fraction of SMW were mostly significant ($p < 10^{-4}$ for all cases except 2013 at 25 m), but varied with decreases (2012) or increases (2013) around 0.1 %. In both years the increase in SGD is an order of magnitude higher than changes in SMW. Thus while SMW is present, we conclude that the freshening trend is being driven primarly by the accumulation of SGD. This process must occur from the top down as SGD is exported in the jet which outflows around 20 m depth (Mankoff et al. 2016; Slater et al. 2018).

Accepted for publication in *Journal of Physical Oceanography*. DOI 10.1175/JPO-D-22-0137.1

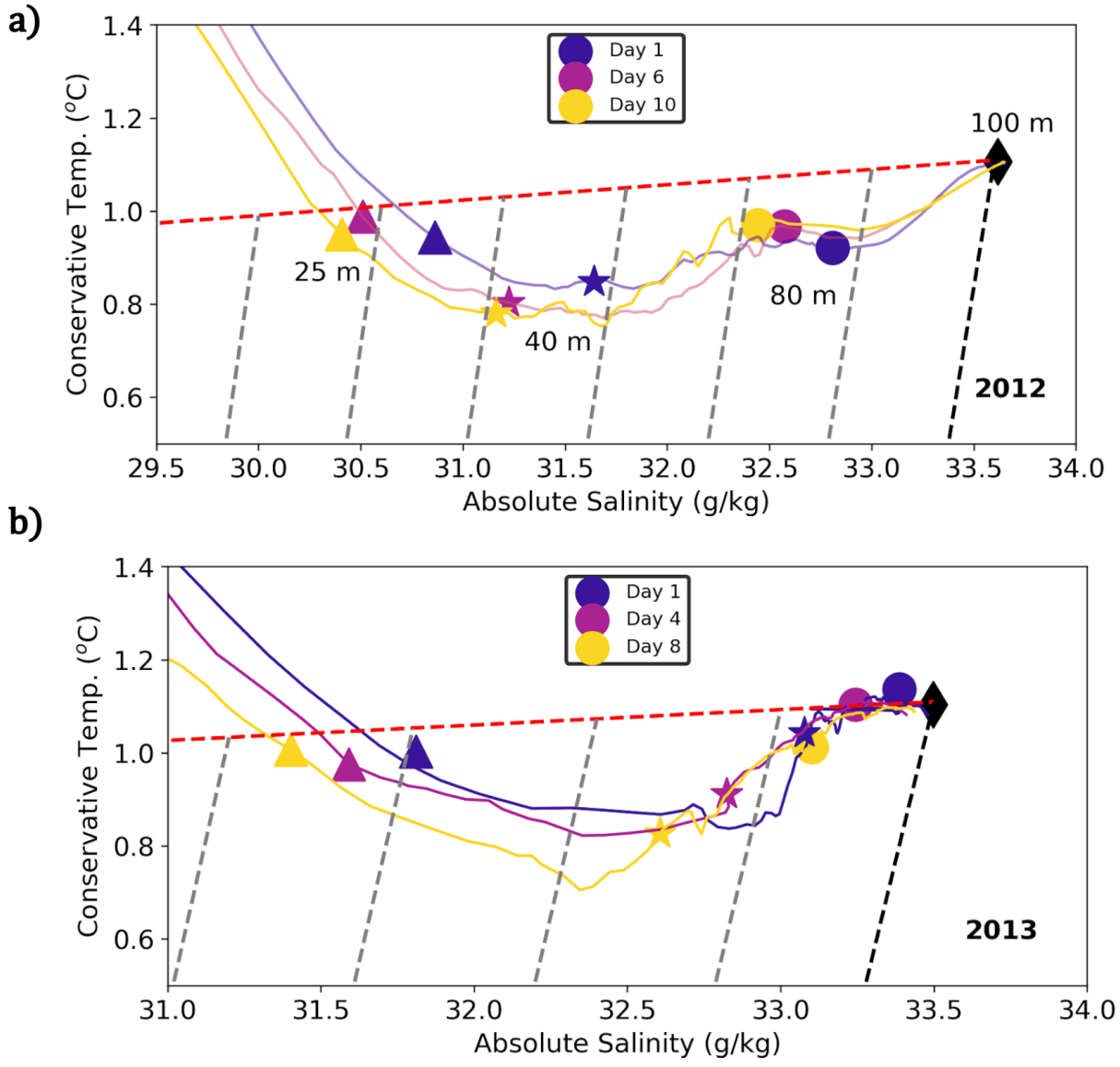

FIG. 4. a) TS diagram of days 1, 4, and 10 in 2012 with the depths 25 (triangles), 40 (stars), 80 (circles) and 100 m (diamond) highlighted with symbols. b) Same as *a* but for 2013, the final point is from day 8 rather than day 10. On top of the TS diagram, we plot a subglacial meltwater discharge-mixing line (red) which represents the mixing between SGD (S = 0 g/kg, Θ = 0 °C) and water at 100 m. There are also submarine melt lines (gray lines), or Gade slopes, which represent a hypothetical mixture of BW and SMW (S = 0, Θ = -87 °C)

d. Interannual Subglacial Meltwater Discharge Differences

Comparison of SGD timeseries from MAR highlights that SGD flux into the fjord was substantially higher in 2012 than in 2013 (Fig. 5). In 2012, the SGD flux into the fjord started about

Accepted for publication in *Journal of Physical Oceanography*. DOI 10.1175/JPO-D-22-0137.1

TABLE 1. Change in freshwater concentration of SGD and SMW from day 1–10 in 2012 and day 1–8 in 2013.

Depth	2012 ΔSMW	2012 ΔSGD	2013 ΔSMW	2013 ΔSGD
25 m	-0.06 ± 0.03 %	1.5 ± 0.2 %	0.02 ± 0.03 %	1.4 ± 0.3 %
40 m	0.08 ± 0.02 %	1.3 ± 0.1 %	0.11 ± 0.05 %	1.0 ± 0.1 %
80 m	-0.08 ± 0.01 %	1.1 ± 0.1 %	0.06 ± 0.03 %	0.4 ± 0.1 %

10 days earlier and the mean flux during the period of sustained SGD (DOY 160–215) was 138 m^3/s compared to 111 m^3/s in 2013 (Fig. 5a). This increased SGD flux resulted in cumulative freshwater input that was 40% higher in 2012 by the end of summer (Fig. 5b). The difference in cumulative SGD grew throughout the summer, such that by the end of the respective field seasons, 0.3 Gt more freshwater had entered in the fjord in 2012 than 2013 (Fig. 5c)

e. Density differences across the outer sill (S2)

Comparison of CTD profiles from inside and outside of SQ shows how the increase in stratification in the inner fjord driven by SGD leads to greater interaction with topography (Fig. 6). In 2012, a density difference arose between the fjord interior and exterior near the depth of S2 (80 m), which separates SQ from TQ. Below this sill depth, the outside profile was less stratified and more dense than profiles within the fjord (Fig. 6a). This feature is not evident in 2013 (Fig. 6b). Note that all profiles have had the linear temporal trend in salinity (Fig. 3) removed so that we can compare profiles taken on different days. Only a single cast was available from outside of the fjord in 2012, and only 2 profiles in 2013, however the density is outside the range of variability observed within the fjord, so the feature is less likely to be transient. The density difference which is centered at the sill depth suggests that as freshening progresses within the inner fjord, the sill can block the export of deep, relatively fresh waters. In 2013, when there was no visible difference between interior and exterior casts, the influence of SGD likely did not extend below S2. The density differences at depth between 2012 and 2013 further support the hypothesis that freshwater is being mixed from the surface downward, as the fjord had both a larger SGD flux and a longer time to accumulate freshwater at depth in 2012.

Accepted for publication in *Journal of Physical Oceanography*. DOI 10.1175/JPO-D-22-0137.1

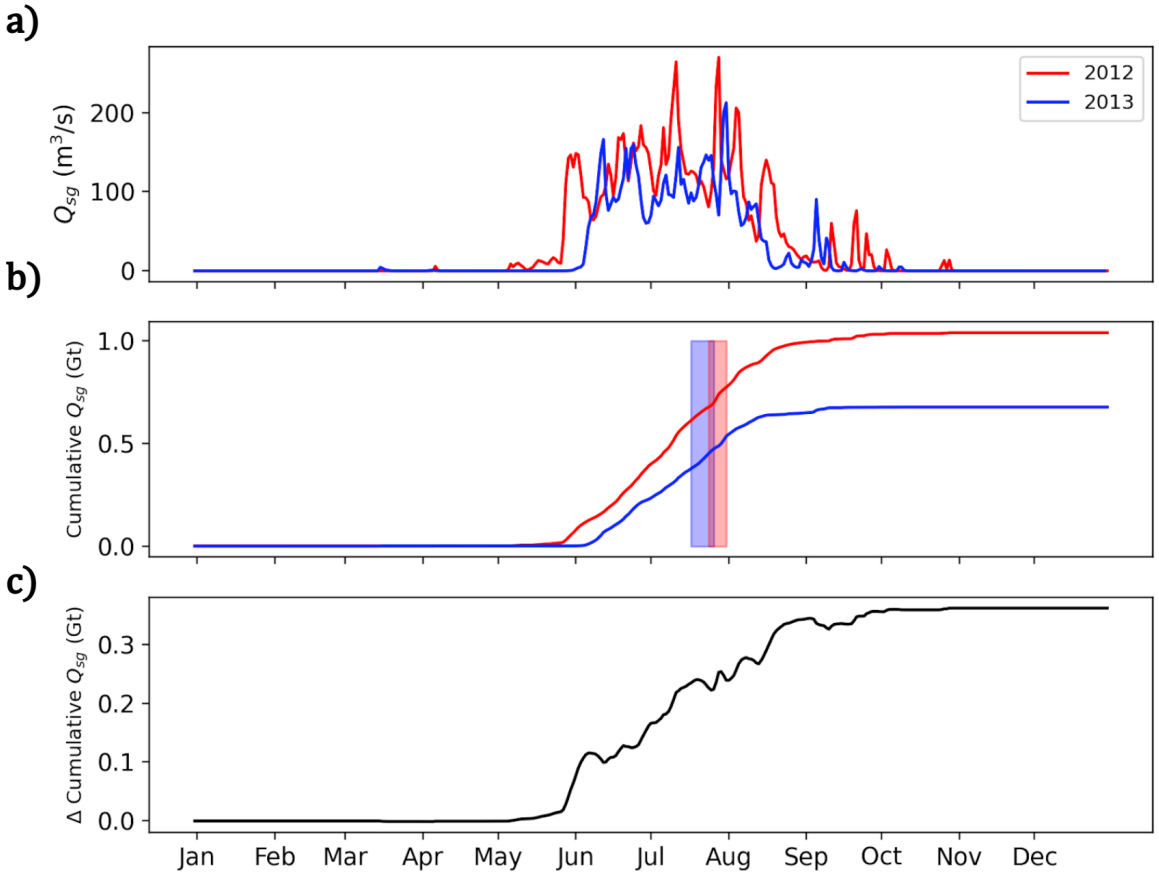

FIG. 5. a) MAR SGD flux into SQ in 2012 and 2013. b) The cumulative SGD given in units of gigatonnes (Gt). Windows are overlaid during the period of the field campaign in 2012 (red) and 2013 (blue) c) The cumulative difference in SGD between 2012 and 2013.

f. Seasonal Change in Circulation

A moored upward-looking ADCP observed fjord circulation for 9 months starting in July 2012, and the changes in circulation were consistent with a seasonal response to freshwater input (Fig. 7). Since the ADCP is located at a single point in an area of recirculation (Fig. 1c; Sup. Fig. 6), it provides an incomplete description of the full circulation. However, it remains the best data available to characterize the seasonal variation in velocity. Additionally, the depth structure of velocity recorded by the ADCP in July is consistent with the snapshot of overturning recorded by across-fjord transects (Sup. Fig. 7–12.), indicating that the ADCP measurements are correlated

Accepted for publication in *Journal of Physical Oceanography*. DOI 10.1175/JPO-D-22-0137.1

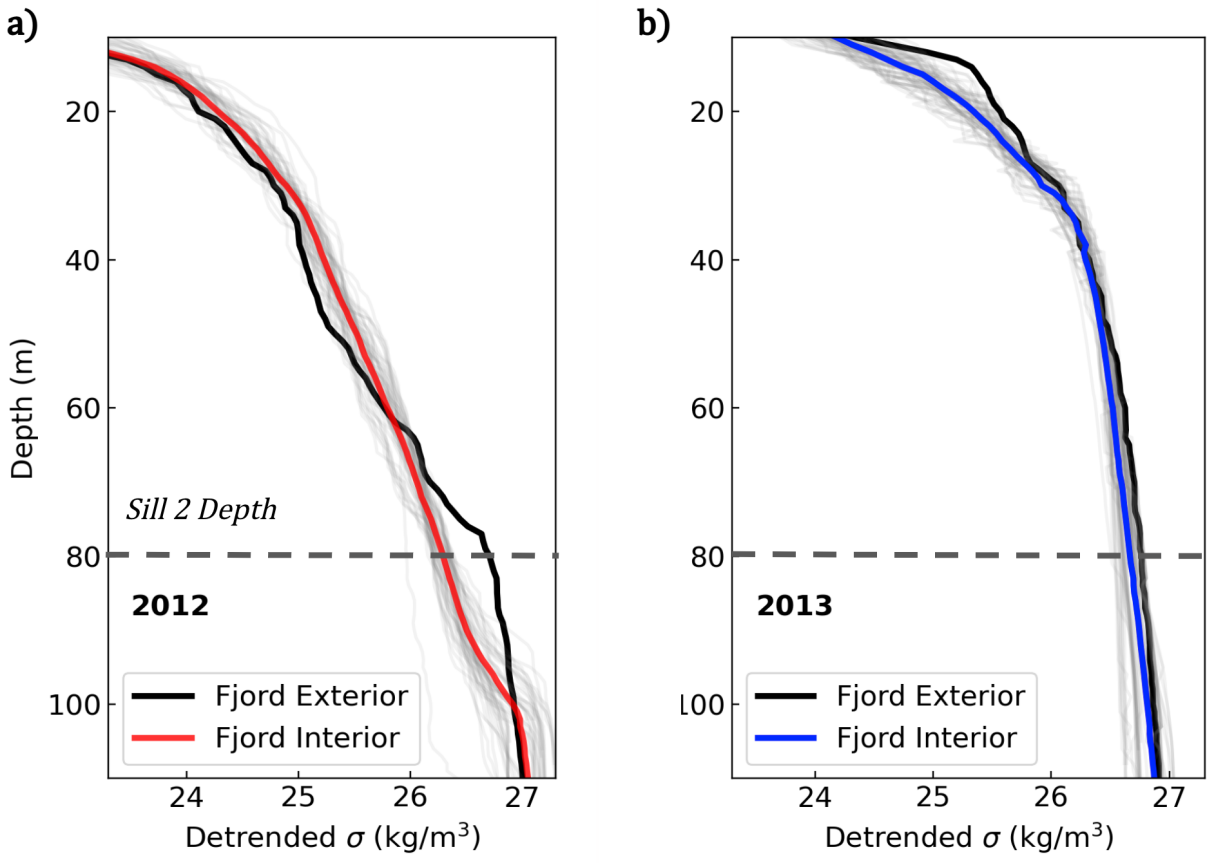

FIG. 6. a) Detrended potential density anomaly for CTD casts in 2012 where the black cast was taken past S2 in Tasiusaq. The dashed line is the depth of S2. b) Same as *a* but for 2013; note that the black cast was calculated using an XCTD.

with the large-scale fjord circulation. Therefore we separate the ADCP velocity into three phases: the plume-driven overturning circulation during the summer, an adjustment period in September, and a weaker phase of circulation after October (Fig. 7a). In July, the outflowing layer was about 30 m thick and centered around 25 m, while the inflowing layer was 40 m thick and centered around the depth of S2, and the basin layer below 100 m had relatively weak velocities (Fig. 7c). During this time period, the plume-driven overturning is clear with the upper layer (25 m) flowing straight out towards the mouth and the middle layer (80 m) flowing in towards the glacier (Fig. 7b). In late August, the estimated SGD flux dropped below 15 m^3/s (10% of peak; Fig. 5) and the upper layer was no longer consistently directed oceanward and there was intermittent flow reversal. In the middle layer however, the flow remained directed towards the glacier, although it was weaker

Accepted for publication in *Journal of Physical Oceanography*. DOI 10.1175/JPO-D-22-0137.1

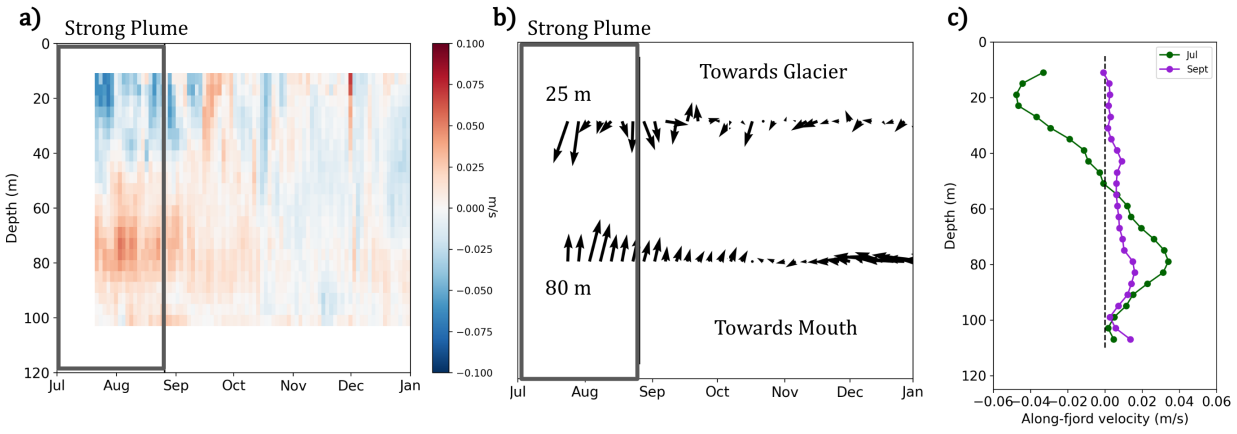

FIG. 7. a) Time series of (2-day running mean) along-fjord velocity from moored ADCP. Negative velocities are directed out of the fjord. The time period when SGD is substantial (> 10% of peak) is outlined in black. b) Directional plot of the (5-day running mean) along-fjord velocity at the depths 25 m (top) and 80 m (bottom). Arrows pointing directly up show flow towards the glacier. West is to the right and the along-fjord velocity is defined positive at 170 degrees from North at this location. c) Vertical profile of along-fjord velocity averaged over the months of July (green) and September (purple).

in magnitude and eventually dropped below 0.005 m/s in October. During this transition period in September, the along-fjord velocity can be described as weak, but steady inflow below 20 m (Fig. 7c). The rapid change in the upper-layer velocity direction suggests that the plume-driven overturning is quickly shut down after SGD weakens, but that a weaker inflow is still present at depth. This weaker exchange flow could be driven by the density gradient between the fjord and S2 (Fig. 6a) that was previously maintained by the plume and recirculation. After October, the lower circulation is weak (< 0.005 m/s) and no longer directed towards the glacier. The time interval between the plume shut down (Q_{sg} < 15 m^3/s) and the shift in circulation to weak velocity is approximately 45 days. Although we lack CTD observations in the fall, Mernild et al. (2015) show a rapid salinity increase in SQ coincident with the shift away from the overturning circulation observed by the ADCP in September.

4. Box Model of Freshwater Storage and Export

We develop a box model to better understand the seasonal variability of fjord circulation and estimate storage of freshwater. The observations imply that under sustained SGD the fjord freshens

Accepted for publication in *Journal of Physical Oceanography*. DOI 10.1175/JPO-D-22-0137.1

(Fig. 3) and that freshwater is mixed downward throughout the summer (Fig. 6) before eventually being exported in the fall (Fig. 7). However, we lack measurements to capture this process continuously and instead rely on observations collected from different years as proxies of different points in the melt season. A box model enables us to explore the dynamics controlling the seasonal cycle and quantify timescales for both freshwater storage and export.

The model is similar in style to previous minimal fjord models in that layer thicknesses and properties evolve according to parameterized exchange with the SGD plume (Zhao et al. 2021) and the external fjord basin (Tasiusaq, Babson et al. 2006; Gillibrand et al. 2013). The model is kept as simple as possible intending to resolve only the first-order dynamics controlling the salinity of the fjord.

a. Box Model Setup

1) Model Layout

We assume the fjord can be described as a three-layer system where the top layer is composed of outflowing glacially-modified water, the middle layer has inflowing water above sill height, and the basin layer has water that is isolated in the deep basin by the sills (Fig. 8). These layers roughly correspond to the observed salinity layers (Fig. 2), and are meant to represent the overturning circulation within the fjord (Fig. 7c). The boxes are forced by a plume at the glacier end and can exchange water in and out of the fjord at the sill 2 (Fig. 8). The fjord has a total depth H and surface area A that is constant with depth. The bottom box represents the waters below sill depth at all times, and therefore we set and hold fixed H_3. Since water is entrained into the plume from this layer, this necessitates the inclusion of an overflow term, Q_O, that represents a flux from the middle layer to the bottom layer. The fjord exterior is assumed to be composed of water with an average salinity S_{ext}.

Temperature is dynamically passive since density gradients are dominated by salinity, and because temperature is relatively homogeneous below 15 m we neglect it from the box model. Submarine melting of the glacier is not included as a freshwater source because it is an order of magnitude smaller than the SGD flux (Table 1) and its omission simplifies the model equations. However in fjords that have large concentrations of icebergs such as Ilulissat Isfjord or Sermilik, SMW would have to be included as a freshening term (e.g. Moon et al. 2018, Bearid et al. 2018).

Accepted for publication in *Journal of Physical Oceanography*. DOI 10.1175/JPO-D-22-0137.1

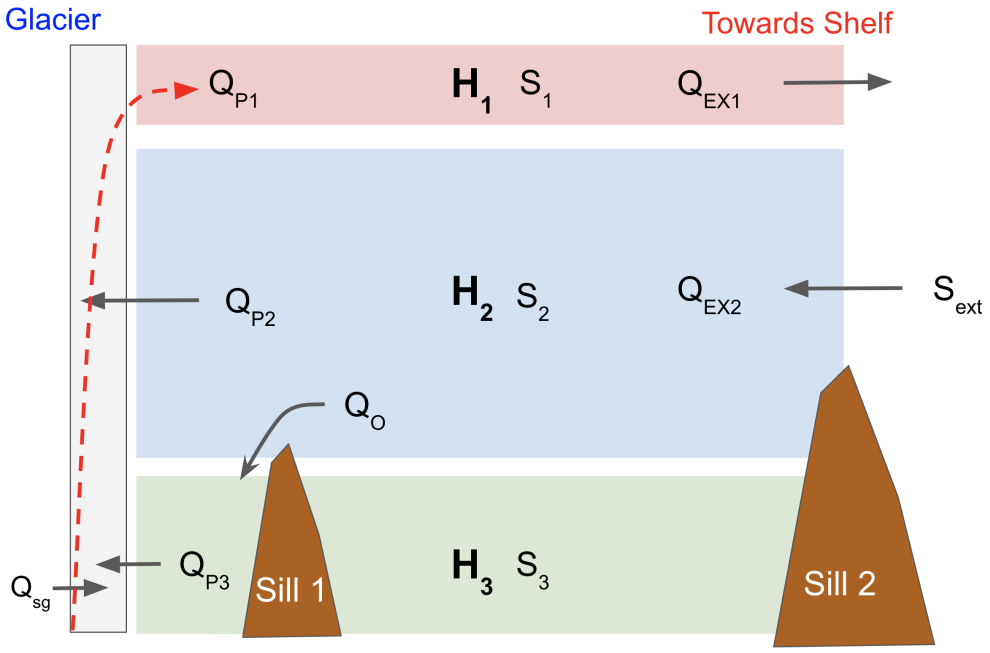

FIG. 8. Schematic of the box model comprising an outflowing upper layer, and inflowing middle layer and a deep passive layer. Layer thickness and salinity is H_j, and S_j respectively where j denotes the layer. Volume flux exchange occurs at the fjord head due to the plume (red) which entrains from the boxes (Q_{Pj}) and at the outer edge due to fjord-shelf density gradients (Q_{EXj}). Sill 1 limits the depth of H_1 and overflow term Q_O is necessary to keep the basin layer volume constant. Sill 2 sets the height of the outflowing layer.

Furthermore, inclusion of submarine melting in the box model was found to have little impact on freshwater storage (Sup. Fig. 11). We wish to keep the model as simple as possible to understand the effects of the primary freshwater source (SGD) so we neglect the effects of sea ice, winds, icebergs and surface forcing. Lastly, the model does not include mixing between layers explicitly, instead mixing is represented through changes in the layer thicknesses which are controlled by the balance between the SGD plume and exchange at the mouth.

2) PLUME TO FJORD EXCHANGE

The effect of SGD is represented through a line plume which entrains ambient water as it rises and then outflows into the upper box H_1. Buoyant plume theory (Jenkins 2011; Straneo and Cenedese 2015) provides analytical expressions for plume volume fluxes, and the volume of ambient water entrained into the plume from the basin layer is given by

Accepted for publication in *Journal of Physical Oceanography*. DOI 10.1175/JPO-D-22-0137.1

$$Q_{P3} = \alpha^{2/3}(g_0')^{1/3} w^{2/3} Q_{sg}^{1/3} H_3, \tag{2}$$

where α is the entrainment coefficient, $g_0' = g\beta_S S_3$ is the reduced gravity of the SGD relative to the basin layer, w is the plume width in the across-fjord direction, Q_{sg} is the SGD and H_3 is the thickness of the basin layer. The volume entrained is therefore determined by the initial buoyancy flux ($g_0' Q_{sg}$) and the height over which the plume rises (H_3). The volume entrained from the middle layer into the plume is similarly given by

$$Q_{P2} = \alpha^{2/3}(g_{P2}')^{1/3} w^{2/3} (Q_{sg} + Q_{P3})^{1/3} H_2, \tag{3}$$

where $g_{P2}' = g\beta_S(S_2 - S_{P2})$ is the reduced gravity of the plume relative to the middle box and the volume flux of the plume entering the middle box has grown to include the entrained water Q_{P3}. The volume flux from the plume into the upper box is then equal to

$$Q_{P1} = Q_{sg} + Q_{P3} + Q_{P2}. \tag{4}$$

We also require expressions for the salinity of the plume as it rises. The salinity of the plume as it enters the middle box is

$$S_{P2} = \frac{Q_{P3} S_3}{Q_{P3} + Q_{sg}}, \tag{5}$$

and the salinity of the plume as it enters box 1 is

$$S_{P1} = \frac{Q_{P3} S_3 + Q_{P2} S_2}{Q_{P3} + Q_{sg} + Q_{P2}}. \tag{6}$$

3) External Fjord Exchange

The volume flux exchange out of the fjord could be parameterized in a number of ways depending on whether the flow is externally-forced (e.g., hydraulic control, wind forcing), or internally-forced, as is typical for estuarine circulation (Sutherland et al. 2014; Zhao et al. 2018, 2021). Zhao et al. (2021) provides scalings for estimating the volume flux at the sill using the density gradient across the sill for hydraulically controlled or relatively wide (geostrophic transport) fjords. Hydraulic

Accepted for publication in *Journal of Physical Oceanography*. DOI 10.1175/JPO-D-22-0137.1

control occurs when the Froude number $Fr = U/c$, a ratio of the advective speed U over baroclinic wave speed c, is greater than 1 at constrictions or sills. Ship-mounted ADCP velocity transects (Fig. S8–S12) show that although $Fr > 1$ close to the glacier within the jet, $Fr < 1$ at the sill so we do not believe hydraulic control to be occurring. We also found the predicted hydraulic control transport (12000 m^3/s) to overestimate transport from a ship-mounted ADCP transect (Sup. Fig. 13 (1900–6700 m^3/s, Sup. Table 2). The importance of geostrophic flow in estuaries can be quantified through the Kelvin number ($Ke = W/L_d$), a ratio of the fjord width over the deformation radius $L_d = c/f$, where c is again the baroclinic wave speed and f is the Coriolis frequency (Carroll et al. 2017; Jackson et al. 2018). In SF, Ke is around 1 in the channel (2 km width) and $Ke > 1$ in the wide basin (5 km width). Therefore, rotational effects are important in the wide basin, but flow within the channel is a combination of vertical and horizontal shear (Valle-Levinson 2008). The predicted geostrophic transport (2600–3600 m^3/s) was similar to an estimate of the gravitational (estuarine) transport (2200 m^3/s), lending support for both approaches. We note that these two theories are not necessarily incompatible with one another. Ultimately, we choose to go with a gravitational parameterization since the primary density gradient we are interested in is produced close to the terminus, rather than across the sill. Therefore we set the exchange flow using a gravitational (estuarine) circulation

$$Q_{EX1} = W U_g \frac{H_s}{2}, \tag{7}$$

where W is the width of the fjord in the channel, U_g is a scalar velocity for the gravitational circulation and $H_s/2$ is half the sill depth and a scale height associated with the gravitational circulation to turn it into a volume flux. Note that we are solving for the volume flux and not for the layer velocity, since U_g is a scalar velocity not the velocity in a specific layer. In this way, a thin layer should be physically associated with a concentrated flux (faster velocity) and a larger layer should be associated with a diffuse flux (slower velocity).

While gravitational circulation is often dominant in shallower estuaries, we believe it is still appropriate for some glacial fjords despite their relatively large depths due to the vigorous mixing occurring within the plume system, along sidewalls or at sills. An estimate for the strength of the gravitational circulation can be derived assuming a balance between the baroclinic pressure

Accepted for publication in *Journal of Physical Oceanography*. DOI 10.1175/JPO-D-22-0137.1

gradient and friction (Geyer and MacCready 2014)

$$U_g = \frac{g\beta_S H_{12}\bar{S}_x}{r}, \tag{8}$$

where $\bar{S}$ is the vertically-averaged salinity over the first two layers, the subscript x denotes an along-fjord gradient and $1/r$ is a frictional time scale. Equation 8 is a modified gravitational circulation where the classical mixing time scale H^2/K_m has been replaced by a frictional time scale $1/r$ due to uncertainty in the source of mixing. The average along-fjord salinity gradient can be rewritten:

$$\begin{aligned} \bar{S}_x &= \frac{1}{L}\left(S_{ext} - \bar{S}\right), \\ &= \frac{1}{L}\left(S_{ext} + \frac{H_1}{H_{12}}(S_2 - S_1) - S_2\right). \end{aligned} \tag{9}$$

where L is the along-fjord length scale, which we have chosen to be the distance from the glacier to the shelf.

Combining equations 7, 8, and 9 gives:

$$\begin{aligned} Q_{EX1} &= \frac{g\beta_S H_{12} H_s W}{2Lr}\left(S_{ext} + \frac{H_1}{H_{12}}(S_2 - S_1) - S_2\right), \\ &= \frac{\Gamma_{EX}}{r}\Delta\bar{S}. \end{aligned} \tag{10}$$

with the salinity gradient ($\Delta\bar{S}$), friction (r) and fjord geometry (Γ_{EX}) controlling exchange with the out of the fjord. The inflowing exchange flow term is defined overall from conservation of volume within the fjord to be

$$Q_{EX2} = Q_{EX1} + Q_{sg} + Q_O. \tag{11}$$

4) Conservation Equations

Using the Boussinesq approximation, we neglect variations in density and approximate mass conservation with volume conservation. The conservation of volume for each of the boxes is given

Accepted for publication in *Journal of Physical Oceanography*. DOI 10.1175/JPO-D-22-0137.1

by the equations

$$A\frac{\mathrm{d}H_1}{\mathrm{d}t} = Q_{P1} - Q_{EX1}, \tag{12}$$

$$A\frac{\mathrm{d}H_2}{\mathrm{d}t} = -Q_{P2} + Q_{EX2}, \tag{13}$$

$$A\frac{\mathrm{d}H_3}{\mathrm{d}t} = -Q_{P3} + Q_O = 0, \tag{14}$$

where the choice $Q_O = Q_{P3}$ ensures the thickness of the deep box does not change. After substituting the volume conservation equations (12,13,14) into salinity conservation equations we arrive at the simplified salinity equations:

$$AH_1\frac{\mathrm{d}S_1}{\mathrm{d}t} = Q_{P1}(S_{P1} - S_1), \tag{15}$$

$$AH_2\frac{\mathrm{d}S_2}{\mathrm{d}t} = Q_{EX2}(S_{ext} - S_2), \tag{16}$$

$$AH_3\frac{\mathrm{d}S_3}{\mathrm{d}t} = Q_O(S_{ext} - S_3). \tag{17}$$

5) Initial Conditions and Forcing

The model is initially set up to resemble SQ in the spring before the melt season. We initially set $S_{ext} = S_1 = S_2 = S_3 = 33.57$ g/kg such that at the start of the melt season the box model is constant in salinity. In the absence of submarine melting, and provided that S_{ext} is also constant in time (an assumption we make for these simple simulations), we then have $S_2 = S_3 = S_{ext}$ throughout the simulation. This choice simplifies the vertically averaged salinity to be

$$\bar{S} = S_{ext} - \frac{H_1}{H_{12}}(S_{ext} - S_1). \tag{18}$$

While this model includes a constant external salinity and constant friction coefficient, versions of the model with time-varying constants gave qualitatively similar results (Sup. Fig. 14). The layer thicknesses are initially set to $H_1 = 2$ m, $H_2 = 98$ m, and $H_3 = 50$ m, which is the height of

Accepted for publication in *Journal of Physical Oceanography*. DOI 10.1175/JPO-D-22-0137.1

sill S1. A minimum thickness of 2 m is required for the top two layers to keep the model stable and ensure that the model always has all three layers present. The box model geometry is chosen to be as close as possible to SQ with $A = 6.26 \times 10^7$ m^2, $W = 2$ km, $H_s/2 = 40$ m and $L = 60$ km. For the plume parameters, $\alpha = 0.13$, $w = 90$ m, and $\beta_S = 0.75 \times 10^{-3}$ kg/g (Jackson et al. 2017). The friction coefficient $r = 0.0012$ 1/s was chosen because it produced the best model fit with the observations. It is hard to compare this friction coefficient with observations, however comparison against a close analog, the diffusivity mixing time scale H_{12}^2/K_m, suggest the value of the coefficient is high (see Supplemental). The relatively high friction may be seen as compensating for the lack of recirculation in the box model.

The model is forced with SGD taken from the regional climate model MAR (Fig. 5; Mankoff et al. (2020)) and we assume a 15% uncertainty (Mankoff et al. 2020). The model is solved by stepping through the conservation equations with a Backwards Implicit Euler scheme using a 0.1 day timestep. The model is run from day 70 to day 365 in each of 2012 and 2013.

b. Model Results

We start with the box model's seasonal evolution and then compare the predicted salinity and salinity trends with observations. As SGD enters the fjord, the exchange out of the fjord is initially weak and so the top layer thickens (Fig. 9a). H_1 thickens earlier in 2012 than 2013 since SGD enters the fjord earlier, but both reach a maximum thickness of about 70 m. The salinity in the upper layer decreases (Fig. 9b) as freshwater is not sufficiently exported. The freshening of the upper layer starts earlier in 2012, but both years reach a minimum in salinity near day 218. As Q_{sg} weakens at the end of summer then the average salinity in the plume grows (Eq. 6) and S_1 starts to level off. Since the reduction in Q_{sg} occurs at a similar time in 2012 and 2013, salinity minimums in S_1 occur at similar times in both years.

As the upper layer gets thicker, the plume has less distance to rise and so less volume is entrained by the plume, decreasing Q_{P1} (Fig. 9c). At the same time, the changes in H_1 and S_1 increase the density gradient between the fjord and external fjord basin resulting in a higher exchange flow Q_{EX1}. H_1 increases until the exchange flow is greater than the inflow from the plume. Ultimately however, Q_{EX1} overtakes Q_{P1} only when Q_{sg} decreases and the plume shuts down. Since the crossing point is tied to Q_{sg}, it also occurs at a similar time in both years.

Accepted for publication in *Journal of Physical Oceanography*. DOI 10.1175/JPO-D-22-0137.1

When Q_{EX1} overtakes Q_{P1} the fjord starts to net export the freshwater that was stored during the melt season Fig. 9c. We can estimate a timescale for this export as the time taken to exchange all water in the upper layer if the exchange is maintained at its maximum value:

$$\tau_{export} = \frac{AH_1(t_{min})}{Q_{EX1}(t_{min})}, \tag{19}$$

where t_{min} is the time when the salinity is minimized and Q_{sg} starts to fall off. In 2012 and 2013, τ_{export} = 48 and 57 days, respectively, which is similar to the 45 day adjustment timescale estimated from changes in the baroclinic circulation in 2012 (Fig. 7).

The box model results compare reasonably well with the $\bar{S}$ measurements from CTD casts collected in 2012 and 2013, with a mean square error (MSE) of 0.61 g/kg that is reduced after taking into account the uncertainty in Q_{sg} (Fig. 10a). The model also predicts an increase in vertically averaged salinity after the plume shuts off that is consistent with the seal observations from Mernild et al. (2015). The modeled magnitude of salinity trend early in the season matches the magnitude of the observations, but suggest that the magnitude of $\mathrm{d}\bar{S}/\mathrm{d}t$ (Fig. 10b) decreases over summer. Taken as whole, the comparisons against observations suggest the box model does a reasonable job of capturing the observed salinity properties given the model's simplicity. Potentially, the model needs a greater sensitivity to Q_{sg}, since $\bar{S}$ is underestimated in 2012 and overestimated in 2013.

c. Freshwater Export

The combined mean salinity of a layer H_{fw} of pure freshwater and a layer $H_{12} - H_{fw}$ of water with salinity S_{ext} is

$$\bar{S}_{fw} = \frac{H_{fw}S_{fw} + (H_{12} - H_{fw})S_{ext}}{H_{12}}, \tag{20}$$

and therefore we could define the pure freshwater volume in the fjord by $V_{fw} = AH_{fw}$, assuming that there is no freshwater below the inner sill. The mean salinity in Eq. 20 is equivalent to $\bar{S}$ (Eq. 18) and so the net freshwater accumulation or export can be be expressed as

$$\frac{\mathrm{d}V_{fw}}{\mathrm{d}t} = A\frac{\mathrm{d}H_{fw}}{\mathrm{d}t} = -H_{12}A\frac{\mathrm{d}\bar{S}}{\mathrm{d}t}\frac{1}{S_{ext}}, \tag{21}$$

Accepted for publication in *Journal of Physical Oceanography*. DOI 10.1175/JPO-D-22-0137.1

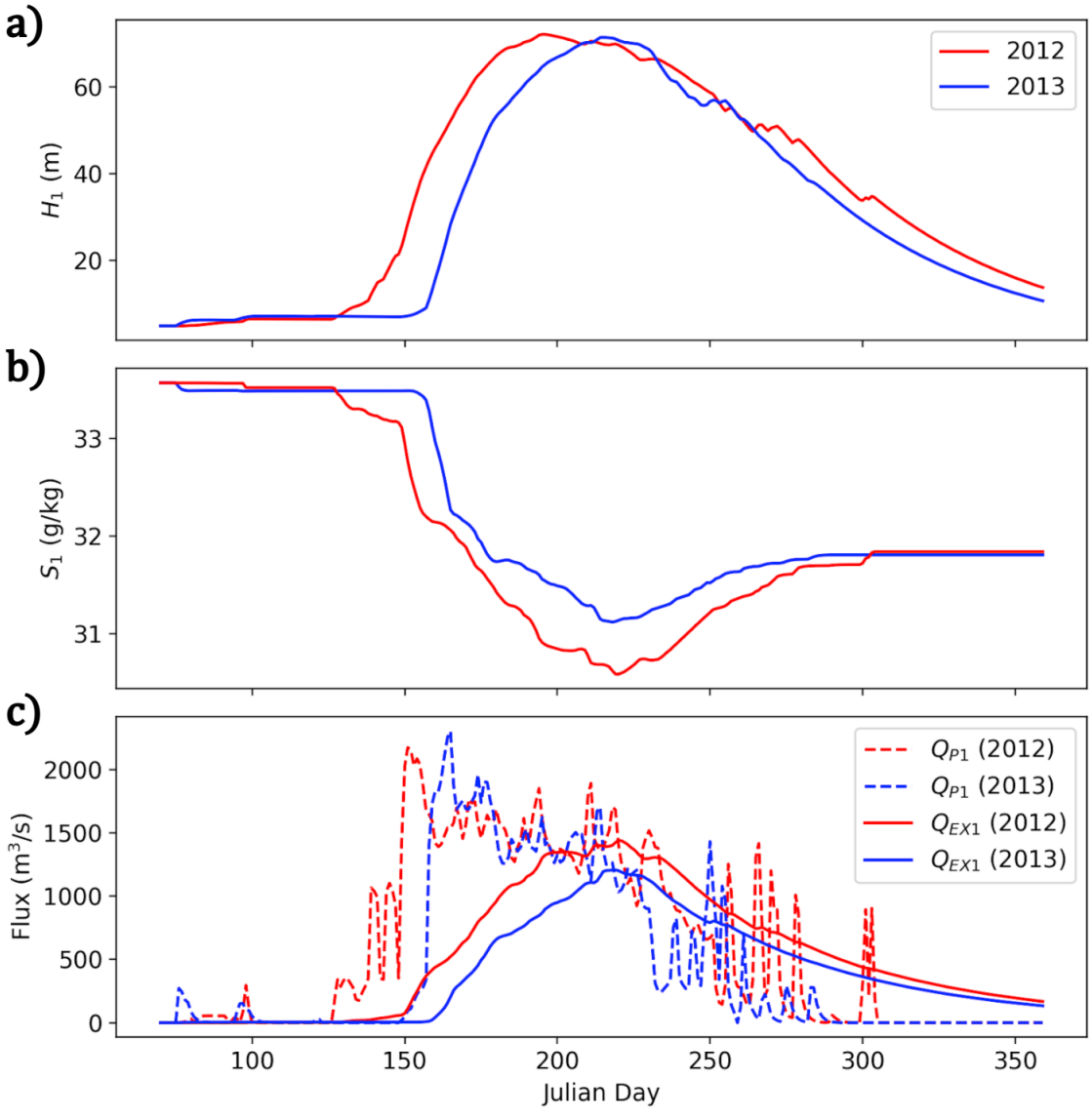

FIG. 9. a) Box model H_1 for 2012 (red) and 2013 (blue) as a function of Julian day. b) same as a, but for S_1. c) Volume fluxes in and out of the top box with dashed lines for the plume fluxes in and solid lines for exchange flow fluxes out.

after rearranging Eq. 20 and taking the derivative. Additionally, since we know the freshwater fluxes into the fjord (Q_{sg}) we can solve for the freshwater flux out of the fjord Q_{fw} through the relation

Accepted for publication in *Journal of Physical Oceanography*. DOI 10.1175/JPO-D-22-0137.1

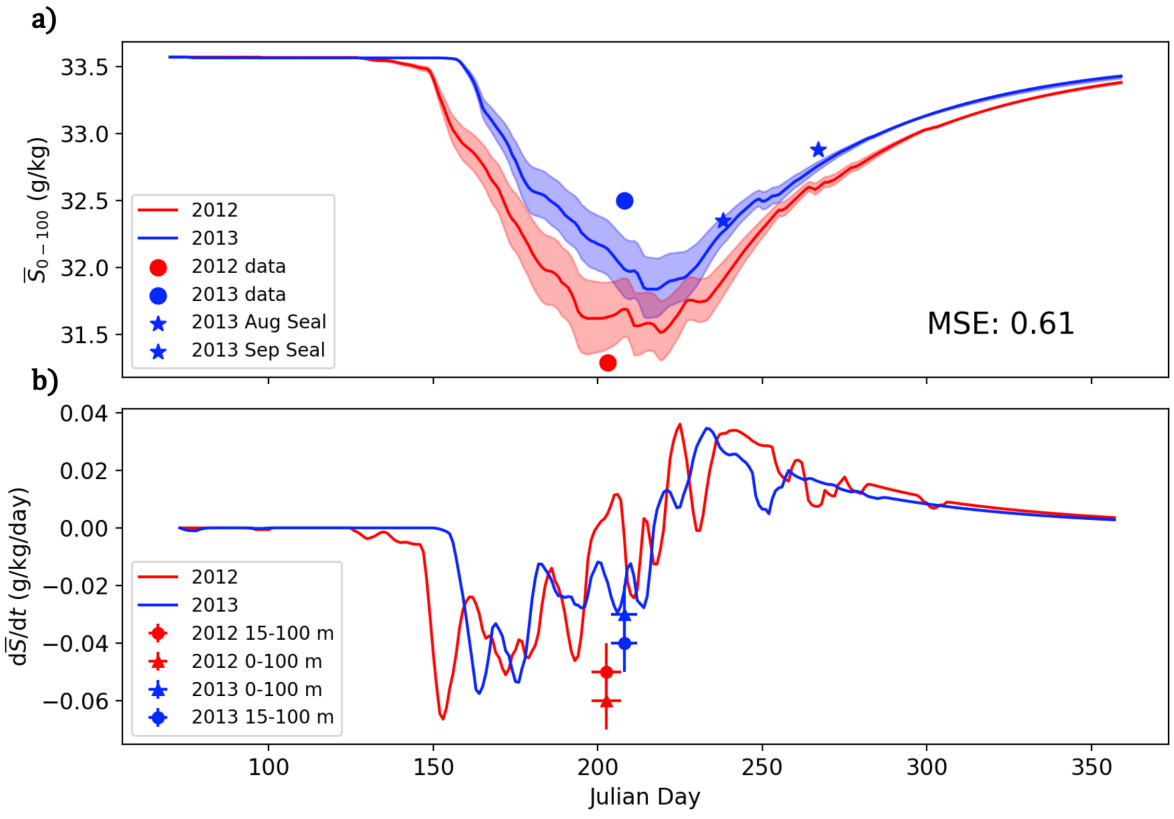

FIG. 10. a) Comparison of the observed vertically averaged salinity ($\bar{S}$) from 0 to 100 m from both the field campaigns and Mernild et al. (2015) seal data against the box model vertically averaged salinity. The shading represents the uncertainty due to SGD flux. b) The derivative of $\bar{S}$ from the box model compared against the observed salinity trends (Fig. 3). The circles are the salinity trend from 15–100 m (Fig. 3) while the triangles are the observed trend from 0–100 m. The horizontal error bars represent the length of the field campaign and vertical error bars represent the uncertainty in the salinity trend. Note the box model does not contain any surface forcing.

$$Q_{fw} = Q_{sg} - \frac{\mathrm{d}V_{fw}}{\mathrm{d}t}. \tag{22}$$

As seen in the box model salinity, the fjord begins to accumulate freshwater once Q_{sg} is non-zero in early summer (Fig. 11a), because the exchange out of the fjord is insufficient to balance the plume fluxes (Fig. 9c, 11b). Freshwater continues to accumulate until it reaches a maximum at 0.3–0.4 Gt around day 218 in both 2012 and 2013. Beyond this, Q_{sg} decreases and the export of freshwater between fjord basins exceeds freshwater input, so that the freshwater volume in the

Accepted for publication in *Journal of Physical Oceanography*. DOI 10.1175/JPO-D-22-0137.1

fjord decays exponentially through the fall (Fig. 11a,b). The peak of Q_{fw} is smaller than the peak magnitude of Q_{sg} because the freshwater flux is distributed over a longer time period. In both years, the peak freshwater fluxes from the fjord are offset from SGD input by about a month (Fig. 11b). The ratio of freshwater stored, $R = 1 - Q_{fw}/Q_{sg}$, shows a roughly linear decrease in freshwater storage with most freshwater stored early in the season, and most exported late in the season (Fig. 11c).

d. Scaling for freshwater storage

We can generalize the results of the box model to other fjord systems by examining the factors controlling the boundary volume fluxes which set the fjord freshwater content. First, we scale the salinity gradient as

$$\overline{S}_x = \frac{V_{fw}}{V_f + V_{fw}} \frac{S_0}{L_S}, \tag{23}$$

where V_{fw} is the volume of freshwater inside the fjord, $V_f = HLW$ is the volume of the fjord, S_0 is a reference salinity and L_S is the length scale of the salinity gradient, which is not necessarily the same as the length scale of the fjord. Noting that $V_f \gg V_{fw}$, we end up with a scaling for the exchange flow from Eq. 10 as

$$Q_{ex} = C_{out} \times \frac{H_s V_{fw}}{2 L L_S r}, \tag{24}$$

where C_{out}=$g\beta_S S_0$ includes all the constants which vary little from fjord to fjord.

Similarly the plume flux can be approximated from Eq. 2 as

$$Q_p = C_{in} \times Q_{sg}^{1/3} H^* + Q_{sg} + Q_{smw}, \tag{25}$$

where $C_{in} = \alpha^{2/3} g'^{1/3} w^{2/3}$ is a constant, $H^* = H_{gl} - H_s/2$ is the height the plume rises before it enters the top box, and Q_{smw} is the submarine meltwater contribution. Noting that Q_{smw} and Q_{sg} are much smaller than the first term (e.g. Mankoff et al. 2016), the ratio of export to storage can be written as

$$R_{stor} = \frac{C_{out} V_{fw} \delta}{C_{in} Q_{sg}^{1/3} L L_S r}, \tag{26}$$

where δ is the height of the outflowing layer ($H_s/2$) over the height of the rising plume (H^*); analogous to the height of the sill over the height of the grounding line. If the grounding line is

Accepted for publication in *Journal of Physical Oceanography*. DOI 10.1175/JPO-D-22-0137.1

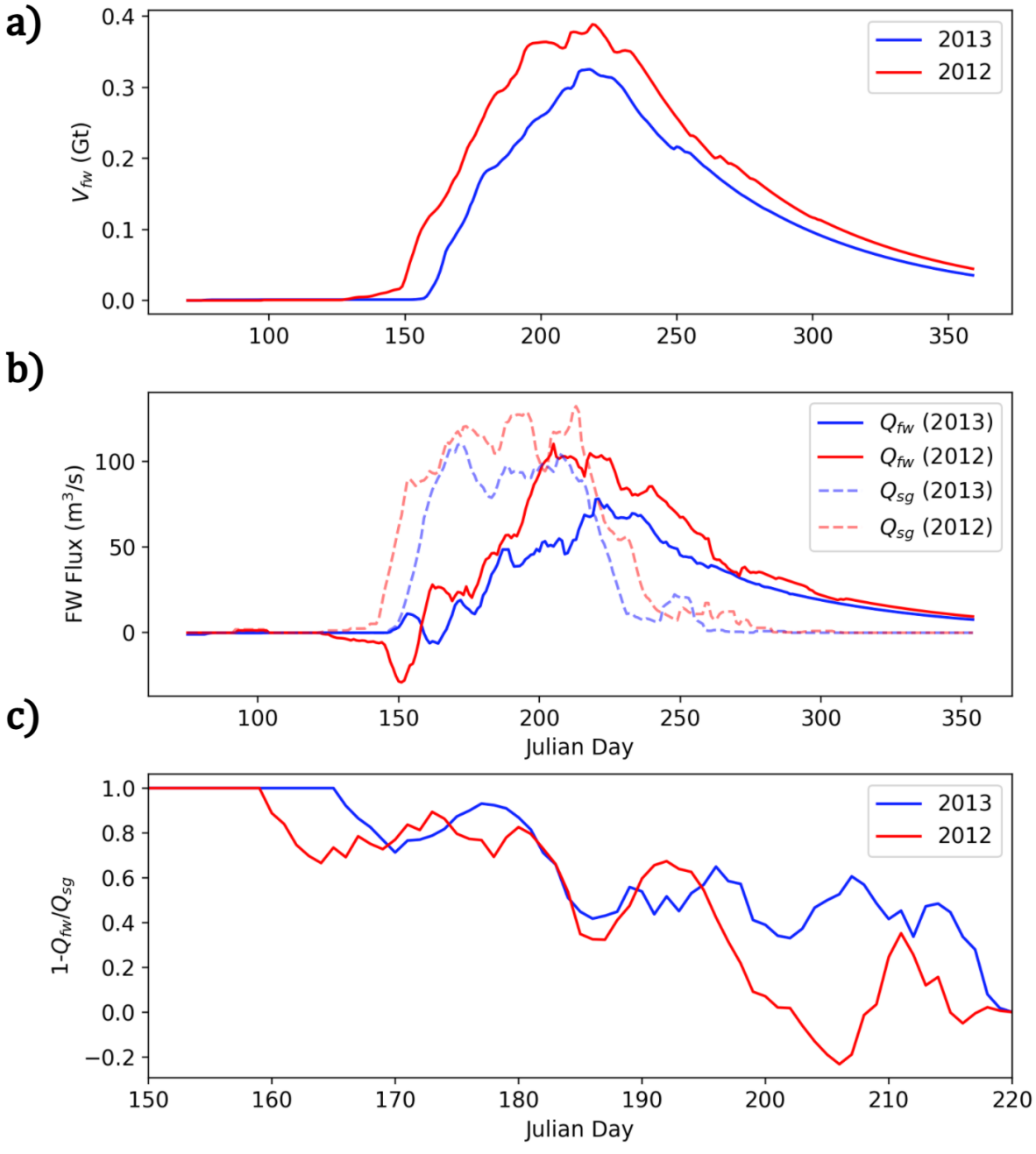

FIG. 11. a) The volume of freshwater (V_{fw}) stored in the box model for 2012 (red) and 2013 (blue) as a function of Julian day. b) Freshwater export (Q_{fw}) from Eq. 22 and SGD (Q_{sg}) in the box model. The a 10-day running mean has been applied to smooth the signal. c) The fraction of SGD that was stored in the fjord during the time period when the plume was active.

Accepted for publication in *Journal of Physical Oceanography*. DOI 10.1175/JPO-D-22-0137.1

the same depth as the sill then δ=1, while realistic examples are δ=0.18 for Ilulissat Isfjord (IL), 0.36 for Saqqarleq (SQ) and 0.73 for Sermilik (SM). From Eq. 26 it is clear that δ is an important parameter controlling freshwater residence time, consistent with Carroll et al. (2017). Additionally, increasing the length of the fjord and the density gradient length scale reduce the exchange flow strength, although for larger systems this increase in storage is likely compensated by a larger total freshwater content (V_{fw}) which increases the density gradient. If friction is dominated by bottom dissipation, then r will be smaller in deeper fjords, but if r is primarily determined by sidewall dissipation or mixing near the plume it might take a similar value from system to system.

We can evaluate how V_{fw} compares across fjord systems under steady state. Initially, the stored freshwater will start out small and all glacial fjords should be in a position where $R_{stor} < 1$. However as V_{fw} increases, a steady state regime will be reached when $R_{stor} = 1$. Using representative values (Table d): we set $R_{stor} = 1$ and get a V_{fw} of 1.9, 0.20, and 2.5 (10^9 m^3) for SM, SQ and IL, respectively, indicating IL will store the most freshwater before exchange is efficient at removing it. However, as a proportion of fjord volume these are 0.004, 0.03, and 0.008 for SM, SQ, and IL which indicates we should expect the greatest changes in mean salinity to occur in SQ. Based on Eq. 26, we see that SQ might be uniquely placed to observe large freshening because it is relatively small and has a moderate sill height compared to grounding line depth. For other systems, such as SM, the combination of a deep sill and large fjord volume may limit the observed freshening. With a known rate of freshwater input (eg, Q_{smw} or Q_{sg}), this threshold V_{fw} could be turned into a residence time. However, these results are based on the assumption that fjord circulation can be described as a gravitational circulation. The exchange of other glacial fjord systems might be primarily wind-driven, geostrophic or hydraulically controlled (e.g. Jackson et al. 2014; Schaffer et al. 2020; Zhao et al. 2021) and so care should be taken in choice of the exchange flow parameterization. Lastly, for systems with significant iceberg cover, we expect iceberg melt to significantly impact the freshwater budget such that it should be accounted for in the box model Moon et al. (2018); Davison et al. (2020).

Accepted for publication in *Journal of Physical Oceanography*. DOI 10.1175/JPO-D-22-0137.1

Fjord	Q_{sg}	L	L_s	V_f	$\delta = H_s/2H^*$
Sermilik	1350 m^3/s	90 km	90 km	5×10^{11} m^3	0.73
Saqqarleq	125 m^3/s	16 km	60 km	7×10^9 m^3	0.36
Ilulissat	1750 m^3/s	50 km	50 km	3×10^{11} m^3	0.18

TABLE 2. Table of values used in the exchange flow scaling for three fjord systems. Q_{sg} is the average SGD in July in 2012 and 2013 (Mankoff et al. 2020). For Sermilik and Ilulissat we assume $L = L_s$ because these systems connect directly with the shelf.

5. Discussion

a. Mechanisms driving freshwater storage

We observe that the mean salinity of SQ decreases during the melt season due to the net accumulation of freshwater. We propose that this process occurs primarily through vertical mixing of SGD. Initially, the density-driven exchange out of the fjord is insufficient at removing freshwater stored near the head, but as the fjord freshens, the exchange flow increases until either the plume shuts off or the fjord reaches steady state. In this section, we discuss these steps in more detail and discuss the possible physical processes contributing to freshwater storage.

The hydrographic observations indicate that the region close to the glacier (< 6 km from the terminus) was accumulating freshwater during the field seasons (Fig. 3) and that the freshening occurred from the surface downward. While submarine melting of glaciers, especially in larger fjords, provides a freshening source at depth, we identify SGD as the primary freshwater being stored. This finding is consistent with independent estimates of freshwater flux into the fjord as Wagner et al. (2019) estimated a combined calving and SMW flux of 0.5 Gt/yr during summer compared to our MAR-estimated SGD flux of 3.5–4.4 Gt/yr during summer.

Using our box model we explored the balance between plume-driven freshwater storage and density-driven freshwater export between fjord basins. Early in the melt season, the exchange out of the fjord is weak and freshwater from the jet is mixed vertically (Fig. 12a). This process deepens the pycnocline within the fjord, akin to H_1 increasing in the model, and is consistent with observed stratification and density profiles of the fjord (Figs. 2, 6). As the pycnocline deepens, the along-fjord density gradient between the fjord and the shelf increases until a crossing point is reached between the tendency for storage and export (Fig. 12b). After the plume shuts down,

Accepted for publication in *Journal of Physical Oceanography*. DOI 10.1175/JPO-D-22-0137.1

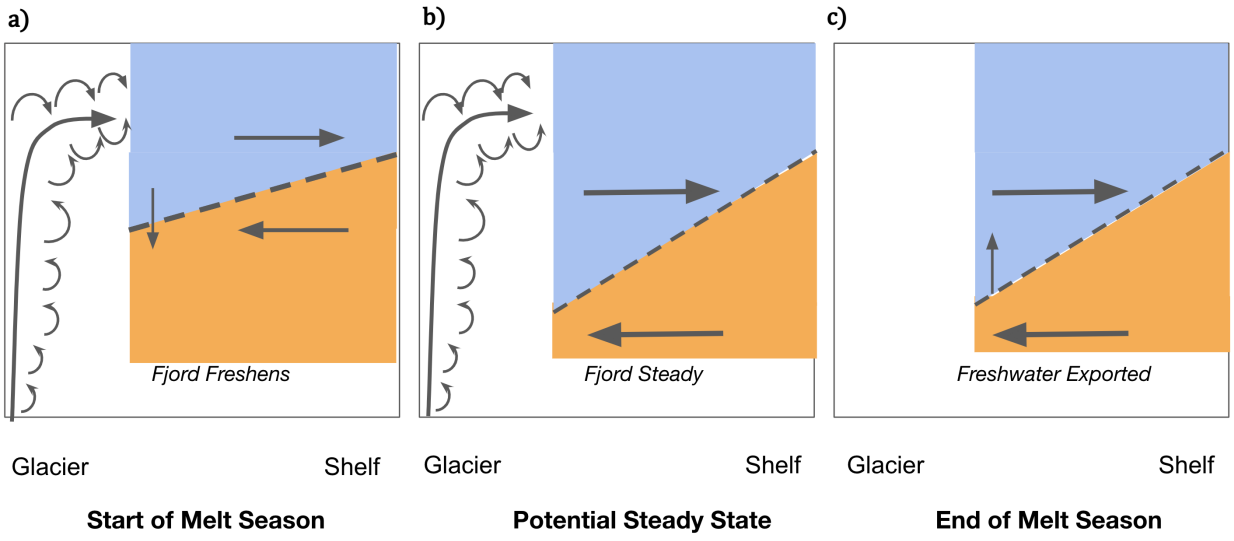

FIG. 12. Schematic of the freshwater storage process. The first panel represents the start of the melt season with mixing near the head of the fjord deepening the pycnocline and relatively weak exchange flow. The middle panel represents a potential steady state that could be reached during the melt season between exchange and mixing within the fjord. The third panel represents the end of the melt season or when mixing tied to the buoyancy-driven circulation weakens and exchange is strong.

freshwater is no longer accumulated and the fjord adjusts through exchange with the external fjord basin over the next 45 days (Fig. 12c). In reality, the along-fjord density gradient is non-linear in space with the majority of the isopycnal gradients occurring close to the glacier (Mankoff et al. 2016), and mixing in the rest of the fjord likely relatively weak, but not negligible (Bendtsen et al. 2021).

In our box model, the mixing of freshwater between layers is not represented explicitly and instead is included in the exchange parameterization through the frictional time scale $1/r$. Although the friction appears physically consistent with shear-driven mixing from the jet (see Supplemental), other possible sources of mixing which could be represented include dissipation along the walls of the fjord or in the lee of a sill. These mixing processes are common in non-glacial fjords (Klymak and Gregg 2004; Staalstrøm et al. 2015) and along sinuous submarine canyons (Wain et al. 2013), and will be intensified in the presence of recirculation. Additionally, small scale mixing from the submarine melting of ice outside of the plume would enhance the background diffusivity, and future field campaigns should be designed to estimate the energy budgets of these systems.

Accepted for publication in *Journal of Physical Oceanography*. DOI 10.1175/JPO-D-22-0137.1

The parameterization could further be improved by representing recirculation which likely acts to increase the residence time of freshwater in the fjord. Recirculation gyres driven by plumes are found in both observations and models to exist near termini in fjord (Carroll et al. 2017; Slater et al. 2018; Zhao et al. 2021) and large scale recirculations in glacial fjords are connected to glacial melt-rates and overturning strength (Zhao et al. 2022). The strong recirculation cell in SQ can potentially contribute to freshwater storage by redirecting SGD away from the export and back into the plume. Although only a snapshot, ADCP transects across the fjord indicate the volume flux in the recirculation gyre was substantially higher than in the main channel and approximately 50% of the main outflow was redirected back towards the plume in 2013.

We propose the stratification of the fjord increased during the summer, in part due to vertical mixing of freshwater. Glacial fjord plumes are energetic and turbulent (Podolskiy et al. 2021), and shear-driven mixing from buoyant jets can take freshwater at the surface (or within the plume itself) and mix it down below the primary export depth. Recently Bendtsen et al. (2021) found that turbulent mixing rates close to the terminus of Store Gletscher were 100 times higher than mixing rates in the rest of the fjord. Additionally, De Andrés et al. (2020) showed that in 2012 the hydrographic properties of the plume-turned-jet were significantly diluted within a few hundred meters of the terminus indicating that there was additional entrainment and mixing by the jet outflow. Velocity transects across SQ (Sup. Figs. 8–12), show that the Froude is greater than 1 in the core of the outflowing jet indicating that the jet was an inertial-driven flow susceptible to strong shear-driven mixing.

Freshwater storage has also been observed in a glacial fjord in LeConte, Alaska due to the outflow plume impinging on the sill and being redirected back towards the glacier (Hager et al. 2022). In that study, a reflux coefficient (Cokelet and Stewart 1985; MacCready et al. 2021) is calculated which quantifies the amount of export that is mixed vertically back towards the glacier. In a more generic box model than the one we have presented, a reflux coefficient that is a function of Q_{sg} could be added to the fjord-exchange parameterization. Tidal flow over the sill is responsible for the intense mixing which leads to the observed freshwater storage in Godthåbsfjord (Mortensen et al. 2011, 2014). Another potential source of mixing includes internal waves which can be generated by the plume when it impinges on the pycnocline or from tidal flow over the sill (Ezhova et al. 2016, 2017; Mortensen et al. 2014; Stuart-Lee et al. 2021). Therefore, sills and regions close to

Accepted for publication in *Journal of Physical Oceanography*. DOI 10.1175/JPO-D-22-0137.1

the terminus are likely mixing "hot spots" that are elevated by SGD plumes and buoyancy-driven circulation (Bendtsen et al. 2021). Lastly, the interior stratification of the fjord could increase due to the compression of isopycnals with no significant interior mixing taking place. In this scenario, the isopycnal layer corresponding to the neutral buoyancy depth of the plume thickens and the isopycnals below and on top of the neutral buoyancy depth get closer together. However, if this was the dominant mechanism of observed freshening, then the profiles would overlap in TS space in contrast to our observations, which indicate mixing with SGD and SMW (Fig. 4).

b. Delayed Freshwater Export

In ocean circulation models that include Greenland Ice Sheet freshwater forcing, the effects of freshwater storage within glacial fjords should be included as the potential lag can be significant. The lag in peak freshwater export, or freshwater residence time, determined from the box model in SQ is about a month. Our estimated timescale of stored freshwater export is faster than in nearby Ameralik fjord (Stuart-Lee et al. 2021) and Godthåbsfjord (Mortensen et al. 2018), but these glacial fjords have strong tidal mixing and are primarily renewed by dense coastal overflows in the winter. However, our timescale of stored freshwater export is similar to the timescale of destratification that occurs in the fall in LeConte, Alaska (Hager et al. 2022).

It is clear that the lag in freshwater export will be determined by the relationship between exchange at the mouth Q_{ex} and the volume flux from the plume Q_p as our scaling showed (Eq. 26). In a system where Q_{ex} is primarily driven by shelf-forcing (e.g. along-shore winds, eddies, coastal trapped waves) then Q_{ex} will be independent of Q_p and freshwater storage will be set by whether the shelf forcing acts to enhance or reverse the buoyancy-driven flow (Giddings and MacCready 2017). If however, Q_{ex} is driven by buoyancy forcing from the glacier, then its value at the mouth will be sensitive to the amount of reflux or recirculation which occurs within the fjord both of which can act to increase freshwater storage. These volume fluxes will also be influenced by fjord geometry. For example, fjords that are narrow and have shallow sills will limit Q_{ex} resulting in a larger delay of freshwater export (Zhao et al. 2021). Given the sensitivity of fjord-shelf exchange to a number of parameters (e.g. tides, winds, iceberg presence, fjord geometry), continental-wide estimates of freshwater export delay will need to be informed by observations of both hydrography and bathymetry from within a large number of Greenland's glacial fjords (Straneo et al. 2019).

Accepted for publication in *Journal of Physical Oceanography*. DOI 10.1175/JPO-D-22-0137.1

c. Applicability to other fjord systems

Due to several factors such as fjord size and the presence of a single oceanic water mass, it is easier to detect freshwater storage in SQ than in other glacial fjords. As shown with Eq. 26, the volumes of larger glacial fjords such as Sermilik or Ilulissat Icefjord reduce the magnitude of observable salinity trends despite greater freshwater fluxes. However, Stuart-Lee et al. (2021) observed freshwater storage and delayed export occuring in Ameralik, a land-terminating glacial fjord in West Greenland. In that study they attributed the freshwater storage to intense tidal mixing at the sill which drew down freshwater from the surface and increased fjord stratification during the summer and into the fall. This process could also be occurring in SQ and future work should aim to quantify the contribution of tidal mixing at the sill versus mixing induced by the plume/jet. We attribute the mixing primarily to physical processes linked with the jet because we observe freshening first near the terminus and then at S2. However, the two mixing processes are likely working together to increase the fraction of freshwater that is stored.

The processes that led to rapid freshening in SQ, including turbulent plumes and glacier-wide recirculation, will be active in all of Greenland's major glacial fjords since they are driven by SGD. Making equivalent observations to those in SQ at large glacier-fjord systems is extremely challenging due to mobile and thick ice mélange, but the downsloping isopycnals observed near the heads of some glacial fjords (Gladish et al. 2014; Jackson and Straneo 2016; Beaird et al. 2015) could be evidence of a vigorous near-terminous circulation. Experiments with additional endmembers, such as noble gases or oxygen, which can be used as meltwater tracers, are needed to confirm the late departure of freshwater in other systems (Beaird et al. 2015, 2017, 2018).

6. Conclusion

Glacial fjord circulation and properties are often described as bi-modal with plume-driven circulation and strong stratification in the summer and a shelf-driven circulation and weak stratification in the winter. This viewpoint overlooks the potentially significant subseasonal variability within fjords and the potential for transient storage of ice sheet freshwater. We find evidence that during the summer, freshwater is stored within Saqqarleq, a mid-sized glacial fjord in west Greenland, resulting in non-steady mean salinity during the melt season. Specifically, observations of salinity collected in SQ show a freshening trend of 0.05 g/kg/day and 0.04 g/kg/day in 2012 and 2013

Accepted for publication in *Journal of Physical Oceanography*. DOI 10.1175/JPO-D-22-0137.1

respectively . The observations suggest that vertical mixing of SGD increases stratification and freshwater content within the fjord when the plume is active. We developed a box model that is forced by SGD at its glacial boundary and a density-driven exchange with at its sill boundary. Competition between these boundary conditions determines whether freshwater is being stored or removed from the fjord. The box model indicates that glacial fjords with intense mixing are inefficient at removing freshwater, resulting in a lag of 25–30 days between the peak SGD entering the fjord and the freshwater export from the fjord. Future work should aim to identify this process in larger glacial fjords and quantify the interior mixing that redistributes freshwater. Our results provide evidence that fjords modulate the timing and magnitude of ice sheet freshwater entering the wider ocean; processes that should be represented in large-scale climate models if we are to better predict the impact of ice sheet meltwater on the ocean.

Accepted for publication in *Journal of Physical Oceanography*. DOI 10.1175/JPO-D-22-0137.1

Acknowledgments. We would like to acknowledge Margaret Lindeman for helpful discussion and suggestions. We acknowledge Clark Richards, Rebecca Jackson, Sarah Das, Jeff Pietro and others for help in collection of the data. RS and FS acknowledge funding from the NSF. DAS acknowledges support from NERC Independent Research Fellowship NE/T011920/1. We would also like to acknowledge the comments of two anonymous reviewers who greatly improved the manuscript.

Data availability statement. Data for 2013 is available through the NSF Arctic Data Center at the following DOIs: 2013 Ship-based ADCP measurements (doi:10.18739/A2P843W9W); 2013 CTD profiles (doi:10.18739/A2B853H78); moored ADCP (doi:10.18739/A2G73753N); pressure data (doi:10.18739/A2M03XZ70). The 2012 Ship-based ADCP and CTD measurements are available through the NOAA National Centers for Environmental Information (NCEI) using NCEI Accession Number 0210572. The subglacial meltwater discharge data is available from Mankoff et al. (2020). Python notebooks to run the box model are available upon request.

References

Arrigo, K. R., and Coauthors, 2017: Melting glaciers stimulate large summer phytoplankton blooms in southwest greenland waters. *Geophys. Res. Lett.*, **44**, 6278–6285, https://doi.org/10.1002/2017GL073583.

Babson, A. L., M. Kawase, and P. MacCready, 2006: Seasonal and Interannual Variability in the Circulation of Puget Sound, Washington: A Box Model Study. *Atmos.–Ocean*, **44**, 29–45, https://doi.org/10.3137/ao.440103.

Bamber, J. L., M. Oppenheimer, R. E. Kopp, W. P. Aspinall, and R. M. Cooke, 2019: Ice Sheet Contributions to Future Sea-Level Rise from Structured Expert Judgment. *Proc. Natl. Acad. Sci.*, **116**, 11 195–200, https://doi.org/10.1073/pnas.1817205116.

Bamber, J. L., R. M. Westaway, B. Marzeion, and B. Wouters, 2018: The land ice contribution to sea level during the satellite era. *Environ. Res. Lett.*, **13**, 063 008, https://doi.org/10.1088/1748-9326/aac2f0.

Accepted for publication in *Journal of Physical Oceanography*. DOI 10.1175/JPO-D-22-0137.1

Beaird, N., F. Straneo, and W. Jenkins, 2015: Spreading of greenland meltwaters in the ocean revealed by noble gases. *Geophys. Res. Lett.*, **42**, 7705–7713, https://doi.org/10.1002/2015GL065003.

Beaird, N., F. Straneo, and W. Jenkins, 2017: Characteristics of meltwater export from jakobshavn isbræ and ilulissat icefjord. *Ann. of Glaciol.*, **58**, 107–117, https://doi.org/10.1017/aog.2017.19.

Beaird, N., F. Straneo, and W. Jenkins, 2018: Export of Strongly Diluted Greenland Meltwater From a Major Glacial Fjord. *Geophys. Res. Lett.*, **45**, 4163–4170, https://doi.org/10.1029/2018GL077000.

Bendtsen, J., J. Mortensen, K. Lennert, and S. Rysgaard, 2015: Heat sources for glacial ice melt in a west Greenland tidewater outlet glacier fjord: The role of subglacial freshwater discharge. *Geophys. Res. Lett.*, **42**, 4089–4095, https://doi.org/10.1002/2015GL063846.

Bendtsen, J., S. Rysgaard, D. F. Carlson, L. Meire, and M. K. Sejr, 2021: Vertical Mixing in Stratified Fjords Near Tidewater Outlet Glaciers Along Northwest Greenland. *J. Geophys. Res. Oceans*, **126**, e2020JC016 898, https://doi.org/10.1029/2020JC016898.

Böning, C. W., E. Behrens, A. Biastoch, K. Getzlaff, and J. L. Bamber, 2016: Emerging impact of greenland meltwater on deepwater formation in the north atlantic ocean. *Nat. Geosci.*, **9**, 523–527, https://doi.org/10.1038/ngeo2740.

Cape, M. R., F. Straneo, N. Beaird, R. M. Bundy, and M. A. Charette, 2019: Nutrient release to oceans from buoyancy-driven upwelling at Greenland tidewater glaciers. *Nat. Geosci.*, **12**, 34–39, https://doi.org/10.1038/s41561-018-0268-4.

Carroll, D., D. A. Sutherland, E. L. Shroyer, J. D. Nash, G. A. Catania, and L. A. Stearns, 2017: Subglacial discharge-driven renewal of tidewater glacier fjords. *J. Geophys. Res. Oceans*, **122**, 6611–6629, https://doi.org/10.1002/2017JC012962.

Carroll, D., and Coauthors, 2018: Subannual and Seasonal Variability of Atlantic-Origin Waters in Two Adjacent West Greenland Fjords. *J. Geophys. Res. Oceans*, **123**, 6670–6687, https://doi.org/10.1029/2018JC014278.

Accepted for publication in *Journal of Physical Oceanography*. DOI 10.1175/JPO-D-22-0137.1

Cokelet, E. D., and R. J. Stewart, 1985: The exchange of water in fjords: The efflux/reflux theory of advective reaches separated by mixing zones. *J. Geophys. Res. Oceans*, **90**, 7287–7306, https://doi.org/10.1029/JC090iC04p07287.

Davison, B. J., T. R. Cowton, F. R. Cottier, and A. J. Sole, 2020: Iceberg melting substantially modifies oceanic heat flux towards a major Greenlandic tidewater glacier. *Nat. Commun.*, **11**, 5983, https://doi.org/10.1038/s41467-020-19805-7.

De Andrés, E., D. A. Slater, F. Straneo, J. Otero, S. Das, and F. Navarro, 2020: Surface emergence of glacial plumes determined by fjord stratification. *Cryosphere Discuss.*, 1–41, https://doi.org/10.5194/tc-2019-264.

Delhasse, A., C. Kittel, C. Amory, S. Hofer, D. van As, R. S. Fausto, and X. Fettweis, 2020: Brief communication: Evaluation of the near-surface climate in ERA5 over the Greenland Ice Sheet. *Cryosphere*, **14**, 957–965, https://doi.org/10.5194/tc-14-957-2020.

Dukhovskoy, D., I. Yashayaev, A. Proshutinsky, J. L. Bamber, I. L. Bashmachnikov, E. P. Chassignet, C. M. Lee, and A. J. Tedstone, 2019: Role of greenland freshwater anomaly in the recent freshening of the subpolar north atlantic. *J. Geophys. Res. Oceans*, **124**, 3333–3360, https://doi.org/10.1029/2018JC014686.

Erofeeva, S., and G. Egbert, 2020: Arc5km2018: Arctic ocean inverse tide model on a 5 kilometer grid, 2018. *Dataset*, https://doi.org/10.18739/A21R6N14K.

Ezhova, E., C. Cenedese, and L. Brandt, 2016: Interaction between a Vertical Turbulent Jet and a Thermocline. *J. Phys. Oceanogr.*, **46**, 3415–3437, https://doi.org/10.1175/JPO-D-16-0035.1.

Ezhova, E., C. Cenedese, and L. Brandt, 2017: Dynamics of a Turbulent Buoyant Plume in a Stratified Fluid: An Idealized Model of Subglacial Discharge in Greenland Fjords. *J. Phys. Oceanogr.*, **47**, 2611–2630, https://doi.org/10.1175/JPO-D-16-0259.1.

Fettweis, X., and Coauthors, 2017: Reconstructions of the 1900–2015 Greenland ice sheet surface mass balance using the regional climate MAR model. *Cryosphere*, **11**, 1015–1033, https://doi.org/10.5194/tc-11-1015-2017.

Frajka-Williams, E., J. Bamber, and K. Våge, 2016: Greenland melt and the atlantic meridional overturning circulation. *Oceanog.*, **29**, 22–33, https://doi.org/10.5670/oceanog.2016.96.

Accepted for publication in *Journal of Physical Oceanography*. DOI 10.1175/JPO-D-22-0137.1

Geyer, W. R., and P. MacCready, 2014: The Estuarine Circulation. *Annu. Rev. Fluid Mech.*, **46**, 175–197, https://doi.org/10.1146/annurev-fluid-010313-141302.

Giddings, S. N., and P. MacCready, 2017: Reverse Estuarine Circulation Due to Local and Remote Wind Forcing, Enhanced by the Presence of Along-Coast Estuaries. *J. Geophys. Res. Oceans*, **122**, 10 184–10 205, https://doi.org/10.1002/2016JC012479.

Gillibrand, P. A., M. E. Inall, E. Portilla, and P. Tett, 2013: A box model of the seasonal exchange and mixing in Regions of Restricted Exchange: Application to two contrasting Scottish inlets. *Environ. Model. Softw.*, **43**, 144–159, https://doi.org/10.1016/j.envsoft.2013.02.008.

Gladish, C. V., D. M. Holland, A. Rosing-Asvid, J. W. Behrens, and J. Boje, 2014: Oceanic boundary conditions for Jakobshavn Glacier. Part I: Variability and renewal of Ilulissat Icefjord Waters, 2001–14. *J. Phys. Oceanogr.*, **45**, 3–32, https://doi.org/10.1175/JPO-D-14-0044.1.

Goelzer, H., and Coauthors, 2020: The future sea-level contribution of the Greenland ice sheet: a multi-model ensemble study of ISMIP6. *Cryosphere Discuss.*, 1–43, https://doi.org/10.5194/tc-2019-319.

Hager, A. O., D. A. Sutherland, J. M. Amundson, R. H. Jackson, C. Kienholz, R. J. Motyka, and J. D. Nash, 2022: Subglacial discharge reflux and buoyancy forcing drive seasonality in a silled glacial fjord. *J. Geophys. Res. Oceans*, **127**, e2021JC018 355, https://doi.org/10.1029/2021JC018355.

Hendry, K. R., N. Briggs, S. Henson, J. Opher, J. A. Brearley, M. P. Meredith, M. J. Leng, and L. Meire, 2021: Tracing Glacial Meltwater From the Greenland Ice Sheet to the Ocean Using Gliders. *J. Geophys. Res. Oceans*, **126**, e2021JC017 274, https://doi.org/10.1029/2021JC017274.

Hopwood, M. J., D. Carroll, T. J. Browning, L. Meire, J. Mortensen, S. Krisch, and E. P. Achterberg, 2018: Non-linear response of summertime marine productivity to increased meltwater discharge around Greenland. *Nat. Commun.*, **9**, 1–9, https://doi.org/10.1038/s41467-018-05488-8.

Hopwood, M. J., and Coauthors, 2020: Review article: How does glacier discharge affect marine biogeochemistry and primary production in the Arctic? *Cryosphere*, **14**, 1347–1383, https://doi.org/10.5194/tc-14-1347-2020.

Accepted for publication in *Journal of Physical Oceanography*. DOI 10.1175/JPO-D-22-0137.1

Inall, M. E., T. Murray, F. R. Cottier, K. Scharrer, T. J. Boyd, K. J. Heywood, and S. L. Bevan, 2014: Oceanic heat delivery via Kangerdlugssuaq Fjord to the south-east Greenland ice sheet. *J. Geophys. Res.: Oceans*, **119**, 631–645, https://doi.org/10.1002/2013JC009295, _eprint: https://onlinelibrary.wiley.com/doi/pdf/10.1002/2013JC009295.

Jackson, R. H., S. J. Lentz, and F. Straneo, 2018: The Dynamics of Shelf Forcing in Greenlandic Fjords. *J. Phys. Oceanogr.*, **48**, 2799–2827, https://doi.org/10.1175/JPO-D-18-0057.1.

Jackson, R. H., and F. Straneo, 2016: Heat, Salt, and Freshwater Budgets for a Glacial Fjord in Greenland. *J. Phys. Oceanogr.*, **46**, 2735–2768, https://doi.org/10.1175/JPO-D-15-0134.1.

Jackson, R. H., F. Straneo, and D. A. Sutherland, 2014: Externally forced fluctuations in ocean temperature at Greenland glaciers in non-summer months. *Nat. Geosci.*, **7**, 503–508, https://doi.org/10.1038/ngeo2186.

Jackson, R. H., and Coauthors, 2017: Near-glacier surveying of a subglacial discharge plume: Implications for plume parameterizations. *Geophys. Res. Lett.*, **44**, 6886–6894, https://doi.org/10.1002/2017GL073602.

Jenkins, A., 2011: Convection-Driven Melting near the Grounding Lines of Ice Shelves and Tidewater Glaciers. *J. Phys. Oceanogr.*, **41**, 2279–2294, https://doi.org/10.1175/JPO-D-11-03.1.

Klymak, J. M., and M. C. Gregg, 2004: Tidally Generated Turbulence over the Knight Inlet Sill. *J.Phys. Oceanogr.*, **34**, 1135–1151, https://doi.org/10.1175/1520-0485(2004)034⟨1135:TGTOTK⟩2.0.CO;2.

Le Bras, I., F. Straneo, M. Muilwijk, L. H. Smedsrud, F. Li, M. S. Lozier, and N. P. Holliday, 2021: How much arctic fresh water participates in the subpolar overturning circulation? *J. Phys. Oceanogr.*, **51**, 955–973, https://doi.org/10.1175/jpo-d-20-0240.1.

MacCready, P., and Coauthors, 2021: Estuarine Circulation, Mixing, and Residence Times in the Salish Sea. *J. Geophys. Res. Oceans*, **126**, e2020JC016 738, https://doi.org/10.1029/2020JC016738.

Mankoff, K. D., F. Straneo, C. Cenedese, S. B. Das, C. G. Richards, and H. Singh, 2016: Structure and dynamics of a subglacial discharge plume in a greenlandic fjord. *J. Geophys. Res.: Oceans*, **121**, 8670–8688, https://doi.org/10.1002/2016JC011764.

Accepted for publication in *Journal of Physical Oceanography*. DOI 10.1175/JPO-D-22-0137.1

Mankoff, K. D., and Coauthors, 2020: Greenland liquid water discharge from 1958 through 2019. *Earth Syst. Sci. Data*, **12**, 2811–2841, https://doi.org/10.5194/essd-12-2811-2020, publisher: Copernicus GmbH.

McDougall, T. J., and P. M. Barker, 2011: *Getting started with TEOS-10 and the Gibbs Seawater (GSW) Oceanographic Toolbox*. SCOR/IAPSO WG127, 28 pp.

Meire, L., J. Mortensen, S. Rysgaard, J. Bendtsen, W. Boone, P. Meire, and F. J. R. Meysman, 2016a: Spring bloom dynamics in a subarctic fjord influenced by tidewater outlet glaciers (Godthåbsfjord, SW Greenland). *J. Geophys. Res. Biogeosci.*, **121**, 1581–1592, https://doi.org/10.1002/2015JG003240.

Meire, L., and Coauthors, 2016b: High export of dissolved silica from the Greenland Ice Sheet. *Geophys. Res. Lett.*, **43**, 9173–9182, https://doi.org/10.1002/2016GL070191.

Meire, L., and Coauthors, 2017: Marine-terminating glaciers sustain high productivity in greenland fjords. *Glob. Change Biol.*, **23**, 5344–5357, https://doi.org/10.1111/gcb.13801.

Mernild, S. H., D. M. Holland, D. Holland, A. Rosing-Asvid, J. C. Yde, G. E. Liston, and K. Steffen, 2015: Freshwater Flux and Spatiotemporal Simulated Runoff Variability into Ilulissat Icefjord, West Greenland, Linked to Salinity and Temperature Observations near Tidewater Glacier Margins Obtained Using Instrumented Ringed Seals. *J. Phys. Oceanogr.*, **45**, 1426–1445, https://doi.org/10.1175/JPO-D-14-0217.1.

Moon, T., D. A. Sutherland, D. Carroll, D. Felikson, L. Kehrl, and F. Straneo, 2018: Subsurface iceberg melt key to Greenland fjord freshwater budget. *Nat. Geosci.*, **11**, 49–54, https://doi.org/10.1038/s41561-017-0018-z.

Morlighem, M., and Coauthors, 2017: BedMachine v3: Complete Bed Topography and Ocean Bathymetry Mapping of Greenland From Multibeam Echo Sounding Combined With Mass Conservation. *Geophys. Res. Lett.*, **44**, 11,051–11,061, https://doi.org/10.1002/2017GL074954.

Mortensen, J., J. Bendtsen, K. Lennert, and S. Rysgaard, 2014: Seasonal variability of the circulation system in a west Greenland tidewater outlet glacier fjord, Godthåbsfjord (64°N). *J. Geophys. Res. Earth Surf.*, **119**, 2591–2603, https://doi.org/10.1002/2014JF003267.

Accepted for publication in *Journal of Physical Oceanography*. DOI 10.1175/JPO-D-22-0137.1

Mortensen, J., J. Bendtsen, R. J. Motyka, K. Lennert, M. Truffer, M. Fahnestock, and S. Rysgaard, 2013: On the seasonal freshwater stratification in the proximity of fast-flowing tidewater outlet glaciers in a sub-Arctic sill fjord. *J. Geophys. Res. Oceans*, **118**, https://doi.org/10.1002/jgrc.20134.

Mortensen, J., K. Lennert, J. Bendtsen, and S. Rysgaard, 2011: Heat sources for glacial melt in a sub-arctic fjord (godthåbsfjord) in contact with the greenland ice sheet. **116**, https://doi.org/10.1029/2010JC006528.

Mortensen, J., S. Rysgaard, K. E. Arendt, T. Juul-Pedersen, D. H. Søgaard, J. Bendtsen, and L. Meire, 2018: Local Coastal Water Masses Control Heat Levels in a West Greenland Tidewater Outlet Glacier Fjord. *J. Geophys. Res. Oceans*, **123**, https://doi.org/10.1029/2018JC014549.

Mortensen, J., S. Rysgaard, J. Bendtsen, K. Lennert, T. Kanzow, H. Lund, and L. Meire, 2020: Subglacial Discharge and Its Down-Fjord Transformation in West Greenland Fjords With an Ice Mélange. *J. Geophys. Res. Oceans*, **125**, e2020JC016 301, https://doi.org/10.1029/2020JC016301.

Mortensen, J., S. Rysgaard, M. H. S. Winding, T. Juul-Pedersen, K. E. Arendt, H. Lund, A. E. Stuart-Lee, and L. Meire, 2022: Multidecadal Water Mass Dynamics on the West Greenland Shelf. *J. Geophys. Res. Oceans*, **127**, e2022JC018 724, https://doi.org/10.1029/2022JC018724.

Motyka, R. J., M. Truffer, M. Fahnestock, J. Mortensen, S. Rysgaard, and I. Howat, 2011: Submarine melting of the 1985 Jakobshavn Isbræ floating tongue and the triggering of the current retreat. *J. Geophys. Res. Earth Surf.*, **116**, https://doi.org/10.1029/2009JF001632.

Muilwijk, M., F. Straneo, D. A. Slater, L. H. Smedsrud, J. Holte, M. Wood, C. S. Andresen, and B. Harden, 2022: Export of Ice Sheet Meltwater from Upernavik Fjord, West Greenland. *J. Phys. Oceanogr.*, **52**, 363–382, https://doi.org/10.1175/JPO-D-21-0084.1.

Nghiem, S. V., and Coauthors, 2012: The extreme melt across the Greenland ice sheet in 2012. *Geophys. Res. Lett.*, **39**, https://doi.org/10.1029/2012GL053611.

Oksman, M., and Coauthors, 2022: Impact of freshwater runoff from the southwest Greenland Ice Sheet on fjord productivity since the late 19th century. *Cryosphere Discuss.*, 1–28, https://doi.org/10.5194/tc-2021-373.

Accepted for publication in *Journal of Physical Oceanography*. DOI 10.1175/JPO-D-22-0137.1

Oliver, H., R. M. Castelao, C. Wang, and P. L. Yager, 2020: Meltwater-Enhanced Nutrient Export From Greenland's Glacial Fjords: A Sensitivity Analysis. *J.Geophys. Res. Oceans*, **125**, e2020JC016 185, https://doi.org/10.1029/2020JC016185.

Padman, L., and S. Erofeeva, 2004: A barotropic inverse tidal model for the Arctic Ocean. *Geophys. Res. Lett.*, **31**, https://doi.org/10.1029/2003GL019003.

Podolskiy, E. A., N. Kanna, and S. Sugiyama, 2021: Co-seismic eruption and intermittent turbulence of a subglacial discharge plume revealed by continuous subsurface observations in Greenland. *Commun. Earth Environ.*, **2**, 1–16, https://doi.org/10.1038/s43247-021-00132-8.

Rysgaard, S., and Coauthors, 2020: An Updated View on Water Masses on the pan-West Greenland Continental Shelf and Their Link to Proglacial Fjords. *Journal of Geophysical Research: Oceans*, **125 (2)**, e2019JC015 564, https://doi.org/10.1029/2019JC015564, URL https://onlinelibrary.wiley.com/doi/abs/10.1029/2019JC015564, _eprint: https://onlinelibrary.wiley.com/doi/pdf/10.1029/2019JC015564.

Schaffer, J., T. Kanzow, W.-J. von Appen, L. von Albedyll, J. E. Arndt, and D. H. Roberts, 2020: Bathymetry constrains ocean heat supply to greenland's largest glacier tongue. **13 (3)**, 227–231, https://doi.org/10.1038/s41561-019-0529-x.

Slater, D. A., F. Straneo, S. B. Das, C. G. Richards, T. J. W. Wagner, and P. W. Nienow, 2018: Localized plumes drive front-wide ocean melting of a greenlandic tidewater glacier. *Geophys. Res. Lett.*, **45**, 12,350–12,358, https://doi.org/10.1029/2018GL080763.

Staalstrøm, A., L. Arneborg, B. Liljebladh, and G. Broström, 2015: Observations of Turbulence Caused by a Combination of Tides and Mean Baroclinic Flow over a Fjord Sill. *J. Phys. Oceanogr.*, **45**, 355–368, https://doi.org/10.1175/JPO-D-13-0200.1.

Stevens, L. A., F. Straneo, S. B. Das, A. J. Plueddemann, A. L. Kukulya, and M. Morlighem, 2016: Linking glacially modified waters to catchment-scale subglacial discharge using autonomous underwater vehicle observations. *Cryosphere*, **10**, 417–432, https://doi.org/https://doi.org/10.5194/tc-10-417-2016.

Straneo, F., and C. Cenedese, 2015: The dynamics of greenland's glacial fjords and their role in climate. *Annu. Rev. Mar. Sci.*, **7**, 89–112, https://doi.org/10.1146/annurev-marine-010213-135133.

Accepted for publication in *Journal of Physical Oceanography*. DOI 10.1175/JPO-D-22-0137.1

Straneo, F., and Coauthors, 2019: The case for a sustained Greenland Ice Sheet-Ocean observing system (GrIOOS). *Front. Mar. Sci.*, **6**, https://doi.org/10.3389/fmars.2019.00138.

Stuart-Lee, A. E., J. Mortensen, A.-S. v. d. Kaaden, and L. Meire, 2021: Seasonal Hydrography of Ameralik: A Southwest Greenland Fjord Impacted by a Land-Terminating Glacier. *J.Geophys. Res. Oceans*, **126**, e2021JC017 552, https://doi.org/10.1029/2021JC017552.

Sutherland, D. A., F. Straneo, and R. S. Pickart, 2014: Characteristics and dynamics of two major Greenland glacial fjords. *J. Geophys. Res. Oceans*, **119**, 3767–3791, https://doi.org/10.1002/2013JC009786.

Tedesco, M., X. Fettweis, T. Mote, J. Wahr, P. Alexander, J. E. Box, and B. Wouters, 2013: Evidence and analysis of 2012 greenland records from spaceborne observations, a regional climate model and reanalysis data. **7**, 615–630, https://doi.org/https://doi.org/10.5194/tc-7-615-2013.

Thornalley, D. J., and Coauthors, 2018: Anomalously weak Labrador Sea convection and Atlantic overturning during the past 150 years. *Nature*, **556**, 227–230, https://doi.org/10.1038/s41586-018-0007-4.

Valle-Levinson, A., 2008: Density-driven exchange flow in terms of the kelvin and ekman numbers. *J.Geophys. Res. Oceans*, **113**, https://doi.org/10.1029/2007JC004144.

Wagner, T. J. W., F. Straneo, C. G. Richards, D. A. Slater, L. A. Stevens, S. B. Das, and H. Singh, 2019: Large spatial variations in the flux balance along the front of a Greenland tidewater glacier. *Cryosphere*, **13**, 911–925, https://doi.org/https://doi.org/10.5194/tc-13-911-2019.

Wain, D. J., M. C. Gregg, M. H. Alford, R.-C. Lien, R. A. Hall, and G. S. Carter, 2013: Propagation and dissipation of the internal tide in upper Monterey Canyon. *J. Geophys. Res. Oceans*, **118**, https://doi.org/10.1002/jgrc.20368.

Wood, M., E. Rignot, I. Fenty, D. Menemenlis, R. Millan, M. Morlighem, J. Mouginot, and H. Seroussi, 2018: Ocean-Induced Melt Triggers Glacier Retreat in Northwest Greenland. *Geophys. Res. Lett.*, **45**, 8334–8342, https://doi.org/10.1029/2018GL078024.

Zhao, K. X., A. L. Stewart, and J. C. McWilliams, 2018: Sill-influenced exchange flows in ice shelf cavities. *J.Phys. Oceanogr.*, **49**, 163–191, https://doi.org/10.1175/JPO-D-18-0076.1.

Accepted for publication in *Journal of Physical Oceanography*. DOI 10.1175/JPO-D-22-0137.1

Zhao, K. X., A. L. Stewart, and J. C. McWilliams, 2021: Geometric Constraints on Glacial Fjord–Shelf Exchange. *J. Phys. Oceanogr.*, **51**, 1223–1246, https://doi.org/10.1175/JPO-D-20-0091.1.

Zhao, K. X., A. L. Stewart, and J. C. McWilliams, 2022: Linking Overturning, Recirculation, and Melt in Glacial Fjords. *Geophys. Res. Lett.*, **49**, https://doi.org/10.1029/2021GL095706.

Accepted for publication in *Journal of Physical Oceanography*. DOI 10.1175/JPO-D-22-0137.1